Structures in $K^{\pm}$-Nucleon Total Cross Sections between 0.9 and 2.4 GeV/c†

R. L. Cool, G. Giacomelli,* T. F. Kycia, B. A. Leontic,‡ K. K. Li, A. Lundby,§ J. Teiger,‖ and C. Wilkin¶
Brookhaven National Laboratory, Upton, New York 11973
(Received 8 October 1969)

Total cross sections of $\pi^{\pm}$ and $K^{\pm}$ on hydrogen and deuterium were measured in a standard transmission experiment in the momentum range 0.9–2.4 GeV/c at 50-MeV/c intervals with statistical precisions in the range of 0.2–1.0%. Cross sections for pure isotopic spin states were obtained using a procedure for the deuterium data which takes into account Fermi motion and the shadow effect. This procedure was tested on the pion data before applying it to kaons. Evidence for the following new structures was found: $Y_0^*(2107)$, $Y_0^*(2344)$, $Y_1^*(1912)$, $Y_1^*(2025)$, $Y_1^*(2255)$, $Z_0^*(1780)$, and $Z_1^*(1900)$.

I. INTRODUCTION

MEASUREMENTS of pion-nucleon total cross sections have in the past led to the discovery of many pion-nucleon resonances.[1,2] Only recently have K-meson beams of sufficient purity and intensity become available to allow a search for strange baryon resonances using the total cross-section method. In the present paper, we describe such a search in the momentum range 0.9–2.4 GeV/c. Preliminary results of this experiment, which was performed at the Brookhaven Alternating Gradient Synchrotron, have already been published,[3] as well as results of a subsequent experiment in which the momentum range was extended to 3.3 GeV/c.[4]

Baryon resonances are detected by two different methods. In one case, the resonance is produced as a compound state when protons are bombarded with mesons. Alternatively, the resonance is produced together with other particles. These two methods are sometimes referred to as formation and production experiments, respectively. In a formation experiment, the search for new resonances is performed by measuring a partial or total cross section as a function of the momentum of the incoming meson. At the resonance energy, the cross sections will show an enhancement, in the best case a peak, sometimes a shoulder.

In general, the measurement of the cross section for an appropriate channel as a function of energy will be more sensitive to the presence of resonance than the measurement of the total cross section; the enhancements will stand out more clearly. On the other hand, the relatively poor intrinsic sensitivity of the total cross sections is largely compensated by the simplicity of the total cross-section measurements and by the high precisions obtainable.

Low-mass resonances are as a rule easy to detect because they usually produce large effects. Higher-mass resonances, however, usually appear as broad and nonprominent structures, often overlapping with one another, so that higher accuracy is required. Systematic errors in the absolute cross-section values can be tolerated only if they are essentially energy-independent, but any effect which may produce a structure must be carefully avoided. In the present experiment, point-to-point errors varied between 50 and 900 μb.

If a structure is found in a total cross-section measurement, the information which it yields includes the mass, width, and height, assuming it is a resonance. The isotopic spin is determined directly only for the pure isotopic spin states π^+p and K^+p, while for the other cases, two cross sections have to be measured, and this involves changing either the incident or target particle. For π mesons it is easy to measure both π^+p and π^-p total cross sections and from them to derive the total cross sections $\sigma_{1/2}$ and $\sigma_{3/2}$ in the pure isotopic spin states. Since an experiment with a neutral K-meson beam is at the moment impractical, for K mesons the simplest solution is to measure the cross section on protons and on neutrons. Unfortunately, the only good neutron target consists of neutrons bound inside the deuteron, so that, in this case, problems of nuclear physics in the deuteron complicate the analysis of the data and limit the accuracy. Another limitation of the total cross-section method is the fact that the interpretation of a structure in the total cross section is usually not unique; such structures may be due not only to a single resonance, but may instead be due to several overlapping resonances, or to a threshold effect or other phenomena (see Sec. VIII).

We shall describe the principle of the measurement in Sec. II, the experimental equipment in Sec. III, the experimental procedure in Sec. IV, corrections and errors in Sec. V, and results in Sec. VI. The deuteron

† Work performed under the auspices of the U. S. Atomic Energy Commission.
* On leave of absence from the University of Bologna, Bologna, Italy.
‡ Present address: Institut za Fiziku Sveucilista, Zagreb, Yugoslavia.
§ Present address: CERN, Geneva, Switzerland.
‖ Present address: CEN Saclay, Gif-sur-Yvette, France.
¶ Present address: University College, London, England.
[1] See, for example, M. N. Focacci and G. Giacomelli, CERN Report No. CERN 66-18, 1966 (unpublished), and references quoted therein.
[2] A. Citron, W. Galbraith, T. F. Kycia, B. A. Leontic, R. H. Phillips, A. Rousset, and P. H. Sharp, Phys. Rev. **144**, B1101 (1966).
[3] R. L. Cool, G. Giacomelli, T. F. Kycia, B. A. Leontic, K. K. Li, A. Lundby, and J. Teiger, Phys. Rev. Letters **16**, 1228 (1966); **17**, 102 (1966).
[4] R. J. Abrams, R. L. Cool, G. Giacomelli, T. F. Kycia, B. A. Leontic, K. K. Li, and D. N. Michael, Phys. Rev. Letters **18**, 1209 (1967); **19**, 259 (1967); **19**, 678 (1967).

analysis is taken up in Sec. VII, and a discussion of the results follows in Sec. VIII.

Several new structures have been found in this experiment; their properties are listed in Table VIII, below, together with the properties of some previously reported resonances.

II. PRINCIPLE OF TRANSMISSION EXPERIMENT

The method used for measuring the total cross sections was that of a standard good geometry experiment.

The beam (Fig. 1), after momentum and mass separation, is defined by a system of scintillation counters and by a Čerenkov counter, which further electronically distinguishes between wanted and unwanted particles. The beam then alternatively passes through a hydrogen, deuterium, or dummy target and converges to a focus at the location of the transmission counters, each of which subtends a different solid angle at the center of the target (Fig. 2). The method is thus to evaluate the partial cross sections σ_i measured by each individual transmission counter and to extrapolate these cross sections to zero solid angle to obtain the total cross section.

The partial cross section σ_i measured by the ith transmission counter is given by

$$\sigma_i=(A/\rho_t LN)\ln(R_0/R), \tag{1}$$

where N is Avogadro's number, A is the atomic weight of the target material, L is the target length, ρ_t is the target density, R_0 is the fraction of beam reaching the ith transmission counter when the dummy target is in place, and R is the same fraction for the full target. The assumptions which are implicit in Eq. (1) are (a) that the dummy target is exactly equivalent to the real targets when they are empty, (b) that the whole system is stable over the time required to alternate from a full target to the dummy one, (c) that there should not be electronics effects arising from the different full and empty counting rates in the transmission counters, and (d) that the energy loss suffered by the K mesons in the full target does not change the absorption probability in the region between the target and the transmission counters. In connection with this last point, there will be a need for a decay correction since lower-energy particles, e.g., those which have traversed the full target, have a higher decay probability than those which have traversed the empty target.

Each of the transmission counters measures the total cross section minus the cross section for having a charged secondary in the solid angle subtended by the ith transmission counter:

$$\sigma_i=\sigma_T-\int_0^{\Omega_i}\frac{d\sigma(\theta)}{d\Omega}d\Omega, \tag{2}$$

where σ_T is the total cross section, Ω_i is the mean solid angle subtended by the counter i, and $d\sigma(\theta)/d\Omega$ is the differential cross section for the emission of at least one charged particle at an angle θ. Most of this cross section will be elastic diffraction.

If $d\sigma(\theta)/d\Omega$ is constant within the small angular region subtended, Eq. (2) reduces to

$$\sigma_i=\sigma_T-(d\sigma/d\Omega)\Omega_i. \tag{3}$$

This assumption may be checked experimentally by plotting σ_i against Ω_i; according to (3), one should obtain a straight line. In practice, (3) is valid neither at very small angles because of multiple Coulomb scattering, nor at larger angles because the diffraction scattering cross section starts to fall off rapidly. Below about 2.0 GeV/c the range of momentum transfers covered by the transmission counters is small, and only the multiple-scattering effect at the smallest counters could be observed. Below this energy there were always at least three counters which showed no multiple-scattering effect, and for which the plot was a straight line within statistical errors. Therefore it was possible to extrapolate the straight line given by Eq. (3) to zero solid angle. Above 2.0 GeV/c the extrapolation line had definite curvature, and Eq. (3) had to be modified by the addition of a term in Ω^2.

III. APPARATUS

A. Beam

This type of experiment requires a medium-intensity and low-contamination beam. Intensity is obtained by accepting K mesons produced at 10° with a large angular acceptance and a relatively large momentum bite, and by using a physically short beam. Low contamination is achieved by means of partial separation with electrostatic separators and subsequent electronic separation with a liquid differential Čerenkov counter.

Figure 1 shows the beam layout at Brookhaven's 30-GeV Alternating Gradient Synchrotron. The experiment was situated in the short branch of the separated beam which has a total length of 38 m; also shown is the long branch which continues undeflected through D_2. The K^- mesons were produced internally in a 1.3-mm-diam×13-mm-long Be wire target at the G10 straight section pointing in the beam direction, which was at 10° to the circulating proton beam. The small dimension of the wire corresponded essentially to a point source of secondary particles. The quadrupole triplet Q_1, Q_2, and Q_3 formed a beam parallel vertically and slightly converging horizontally. Particles of the desired momentum were deflected 6° by D_1 into two 15-ft-long electrostatic separators with crossed magnetic field having a vertical aperture of 4 in. and a horizontal aperture of 10 in. The voltage on the gap was maintained at between 400 and 430 kV. The angular acceptance of the beam is defined to be $\Delta\theta_V=\pm 9$ mrad and $\Delta\theta_H=\pm 14$ mrad by a collimator be-

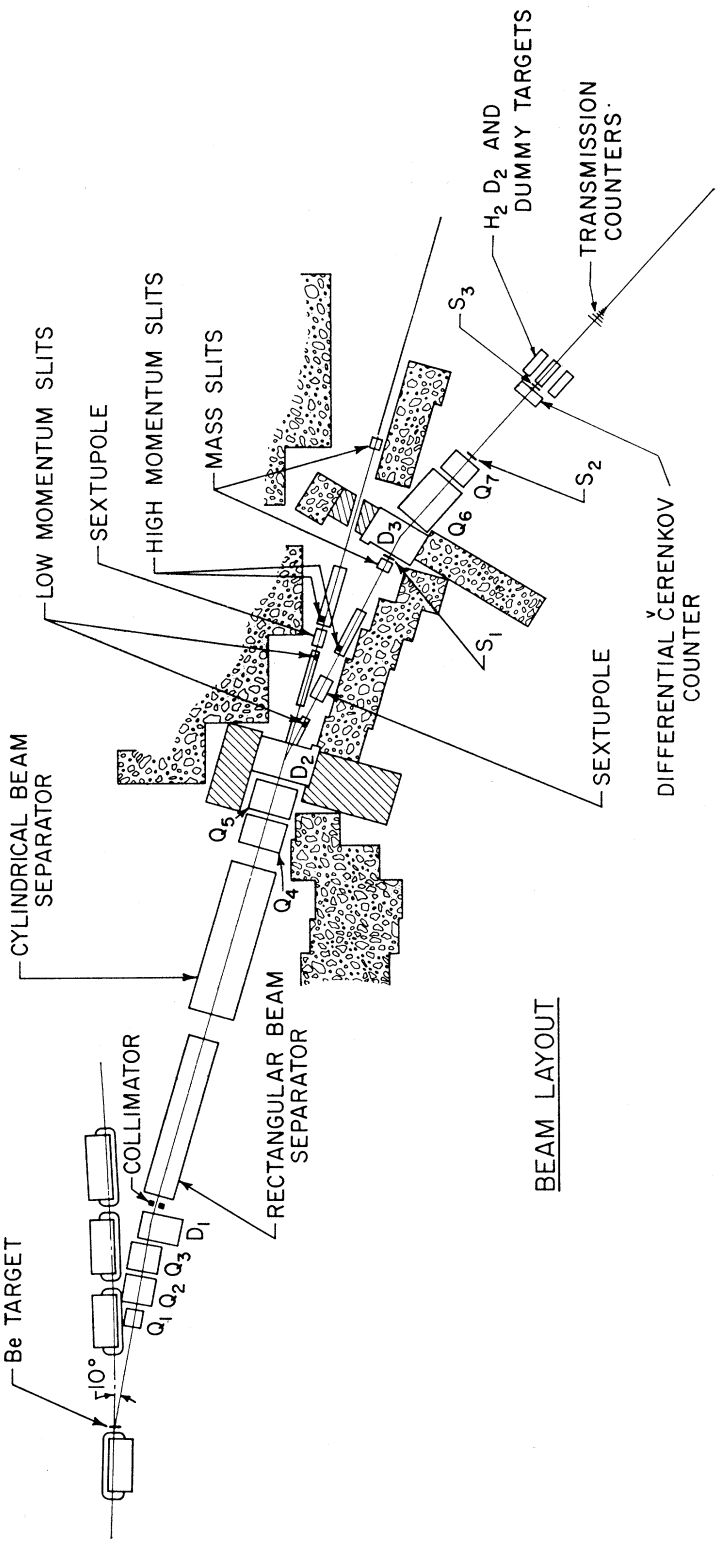

FIG. 1. Layout of partially separated kaon beam. Q_1–Q_7 are quadrupoles, D_1–D_3 bending magnets.

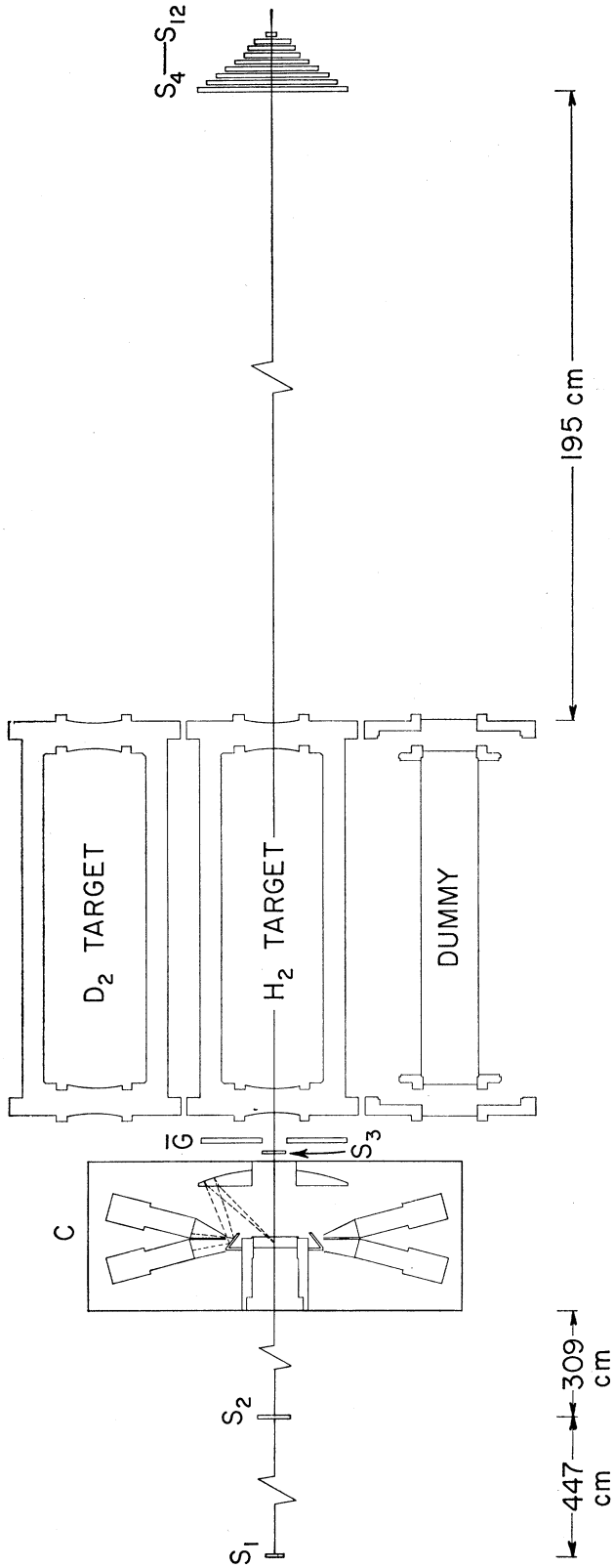

FIG. 2. Layout of experimental apparatus. S_1–S_{12} and $\bar{G}$ are scintillation counters; C is a liquid differential Čerenkov counter; D_2, H_2, and dummy are the liquid deuterium, hydrogen, and empty targets, respectively.

tween D_1 and the first beam separator. The quadrupole doublet Q_4 and Q_5 focused the beam horizontally at the sextupole and vertically at the mass slit. Magnet D_2 provided the necessary deflection for the short branch. The momentum spread in the beam was set at $\Delta p/p = \pm 1.0\%$ by means of Hevimet (tungsten) slits upstream (for -1.0%) and downstream (for $+1.0\%$) from the sextupole at the horizontal images. The sextupole corrected to some extent the chromatic aberrations in the beam. The mass slit, which was made of Hevimet, had a vertical aperture of 0.14 in. and a horizontal aperture of 8 in. The vertical beam size at the mass slit was about 0.090 in. full width at half-height. The separation between K and π images was 0.18 in. at 1.9 GeV/c. When running at high beam intensity, the separators were set to yield the highest K-meson–to–π-meson ratio. The separators, when tuned to K mesons, remove π mesons by a factor of about 100 at 1.9 GeV/c.

Bending magnet D_3, which deflects the beam by 13.5°, recombines momenta and removes the low-momentum components produced at the mass slit. The quadrupole doublet Q_6 and Q_7 forms the final image which is about 1.5 in. vertically and 2 in. horizontally at the transmission counters.

A special snout coupled the vacuum system of the beam to that of the machine with only 0.0005-in.-thick Mylar windows isolating them. The vacuum system extended to the mass slit beyond which helium bags were used. Typical π-to-K ratios of 3 were achieved for the positive beam and 4 for the negative one. Figure 3 shows the actual K-meson fluxes that were obtained in this experiment.

B. Counters

The positions of the counters are shown in Fig. 2, and Table I gives a list of counter dimensions and functions. The K mesons were selected electronically

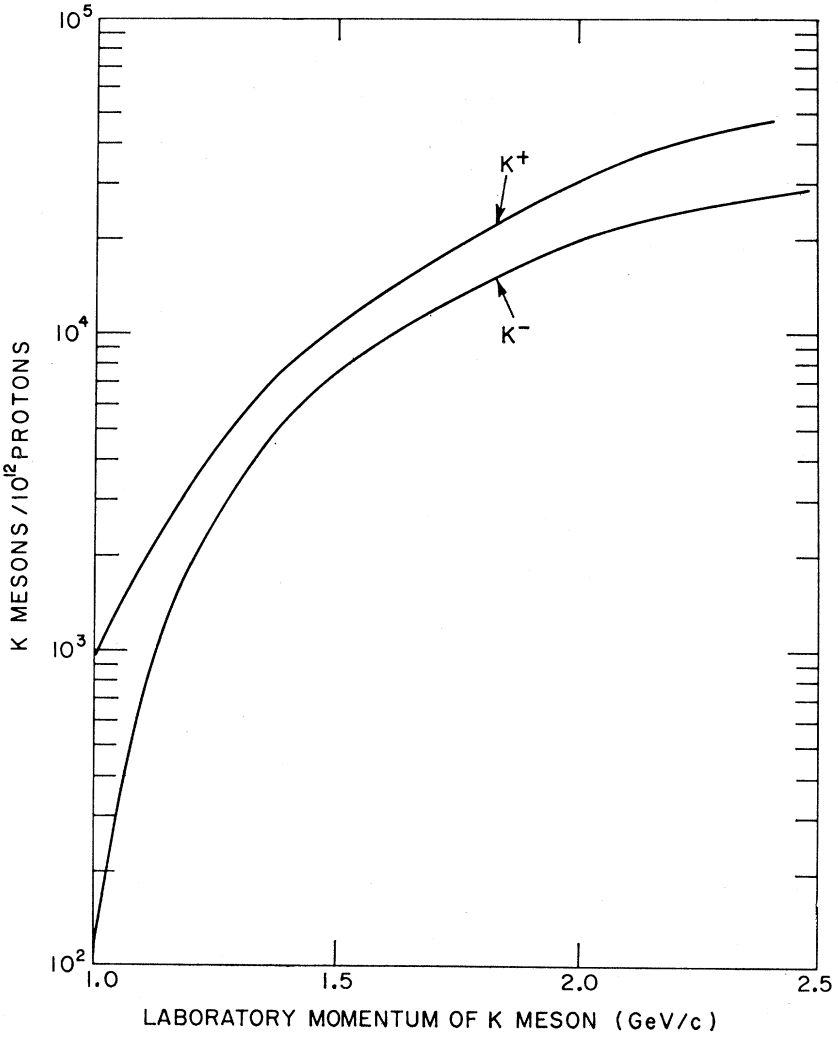

FIG. 3. Kaon beam intensities at the Čerenkov-counter position as function of beam momentum.

TABLE I. Counter dimensions.

Counter	Dimensions (in.)	Thickness (in.)	Function
S_1	8.0×0.31	0.12	Beam counter
S_2	3.25×4.25	0.10	Beam counter
C	5.0 diam	3 cm	Liquid differential Čerenkov counter
S_3	2.5 diam	0.1	Beam counter
$\bar{G}$	2.5 diam hole	0.5	Beam counter
S_4	16.0 diam	0.5	Transmission counter
S_5	14.0 diam	0.5	Transmission counter
S_6	12.0 diam	0.5	Transmission counter
S_7	10.0 diam	0.5	Transmission counter
S_8	8.0 diam	0.5	Transmission counter
S_9	6.0 diam	0.5	Transmission counter
S_{10}	5.0 diam	0.5	Transmission counter
S_{11}	4.0 diam	0.5	Efficiency counter
S_{12}	1.0 diam	0.5	Focusing counter

by the counter combination $S_1S_2S_3\bar{G}\,C\bar{C}$. S_1, S_2, and S_3 are three scintillation counters defining the beam and $\bar{G}$ is a scintillation counter which has a hole the same size as S_3. $\bar{G}$ is used in anticoincidence with S_1, S_2, and S_3 in order to remove halo effects due to particles which surround the main beam. C and $\bar{C}$ are, respectively, the coincidence and anticoincidence outputs of the liquid differential Čerenkov counter,[5] which is needed to give the final selection of K mesons from other particles. The 3-cm-thick cell was filled with perfluorodimethylcyclobutane (C_6F_{12}), which has an index of refraction $n=1.262$ and a density $\rho=1.67$ g cm^{-3}.

In Fig. 2 the principle of the differential counter is shown: Čerenkov light emitted from the radiator is focused by the spherical mirror into slits in front of the photomultipliers after being deflected through 45° by the toroidal mirror. Light from particles with the correct β goes to the coincidence ring, while light from faster particles goes to the anticoincidence ring. Each ring is viewed by nine RCA 8575 photomultipliers. Tuning to particles of different β is achieved by moving the slit and the photomultipliers along the beam direction by means of a remotely controlled electric motor.

The transmission counters S_4–S_{10} were circular scintillation counters, 0.5 in. thick, subtending solid angles at the center of the target ranging from 1.9 to 21 msr. The minimum size of the transmission counters was chosen by requiring that it should encompass all of the unscattered beam. The presence of many counters covering a relatively wide angular range allowed one to check the extrapolation procedure. In the final extrapolation only those counters which showed no multiple-scattering effects were used. The transmission counters were arranged along the beam direction in order of decreasing radius.

Scintillation counter S_{11} was used for checking the efficiency of the transmission counters. Scintillation counter S_{12} was used for beam tuning.

[5] B. A. Leontic and J. Teiger, Brookhaven National Laboratory Internal Report No. BNL-50031 (T-447), 1966 (unpublished).

C. Electronics

The block diagram of the electronics is shown in Fig. 4. Standard Brookhaven National Laboratory nanologic electronics was used. Beam scintillation counters S_1, S_2, S_3, and $\bar{G}$ are taken in coincidence-anticoincidence to form the S output which counts the total beam flux. The outputs of the nine photomultipliers viewing the coincidence ring of the Čerenkov counter are added in three groups of three by passive resistive adders and then taken in threefold coincidence (C). The outputs of the nine photomultipliers viewing the anticoincidence ring are added in a resistive network and provide the anticoincidence signal $\bar{C}$. The total beam output S and Čerenkov-counter output $C\bar{C}$ are taken in coincidence to give the incoming K signal ($K\equiv SC\bar{C}$). This K-meson signal is then taken in coincidence with each of the individual transmission counters, and each coincidence is scaled separately.

The velocity distribution of the beam particles after electrostatic mass separation may be measured by counting ($SC\bar{C}/S$) versus the axial slit position in the differential Čerenkov counter. If the beam separators are tuned to K mesons, one obtains the solid curve of Fig. 5 in the case of a positive beam at 1.30 GeV/c. The graph indicates that at this momentum the π mesons can easily be distinguished from the K mesons and that the number of π mesons present in the beam is about three times the number of K mesons. In order to determine the efficiency of the counter and the π-meson contamination when the counter is set for detecting K mesons, the separators were tuned to π mesons. In this case the beam is not expected to have any measurable contamination of heavier particles and the ($SC\bar{C}/S$) counting rate at the π-meson peak position should give directly the efficiency of the counter. The dotted curve of Fig. 5 was taken in this condition; it indicates that the counter efficiency is about 85%. The ratio of the rate at the K-meson peak position with the beam separators tuned to π mesons to that of them tuned for K mesons gives an upper limit to the π-meson contamination in the actual K-meson experimental run: It is less than 10^{-3}. The separation between π-meson and K-meson peaks became smaller with increasing momentum, but one could always find a good K-meson plateau at which to set the counter.

D. Targets

A sketch of the hydrogen target is shown in Fig. 6. The deuterium and hydrogen targets, built by CRYENCO (Denver, Colo.), were identical. The dummy was similar but not identical; it consisted of a duplicate of the inner target vessel mounted on a frame similar to the vacuum jacket and was not evacuated.

The outer jacket contained liquid hydrogen connected to a large reservoir (285 liters). The vapor pressure in this system was kept at 18.0 psi (1.266 kg/cm^2), corresponding to a temperature of 20.97°K.

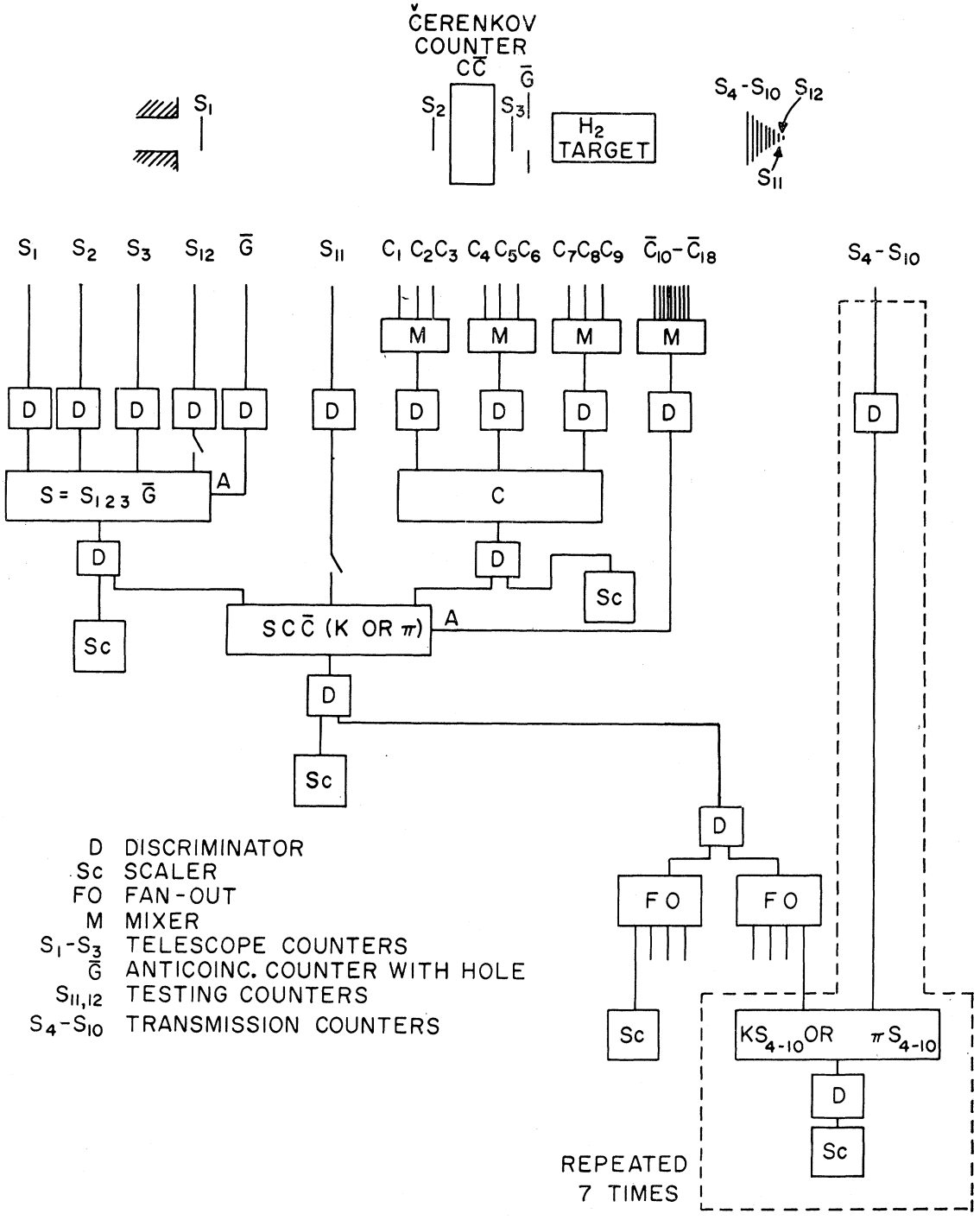

FIG. 4. Block diagram of electronics.

The inner container, which constitutes the target proper, is in thermal contact with the outer jacket. It was filled with gaseous hydrogen (or deuterium) which subsequently liquefied. The temperature of the inner target was taken to be the same as that of the outer one. Its vapor pressure was continuously monitored and found to be constant within ± 0.07 psi. This pressure fluctuation corresponds to a density fluctuation of $\pm 0.05\%$ for hydrogen and deuterium. Absolute uncertainty in the density is probably $\pm 0.05\%$ for hydrogen and should be less than $\pm 0.25\%$ for deuterium.

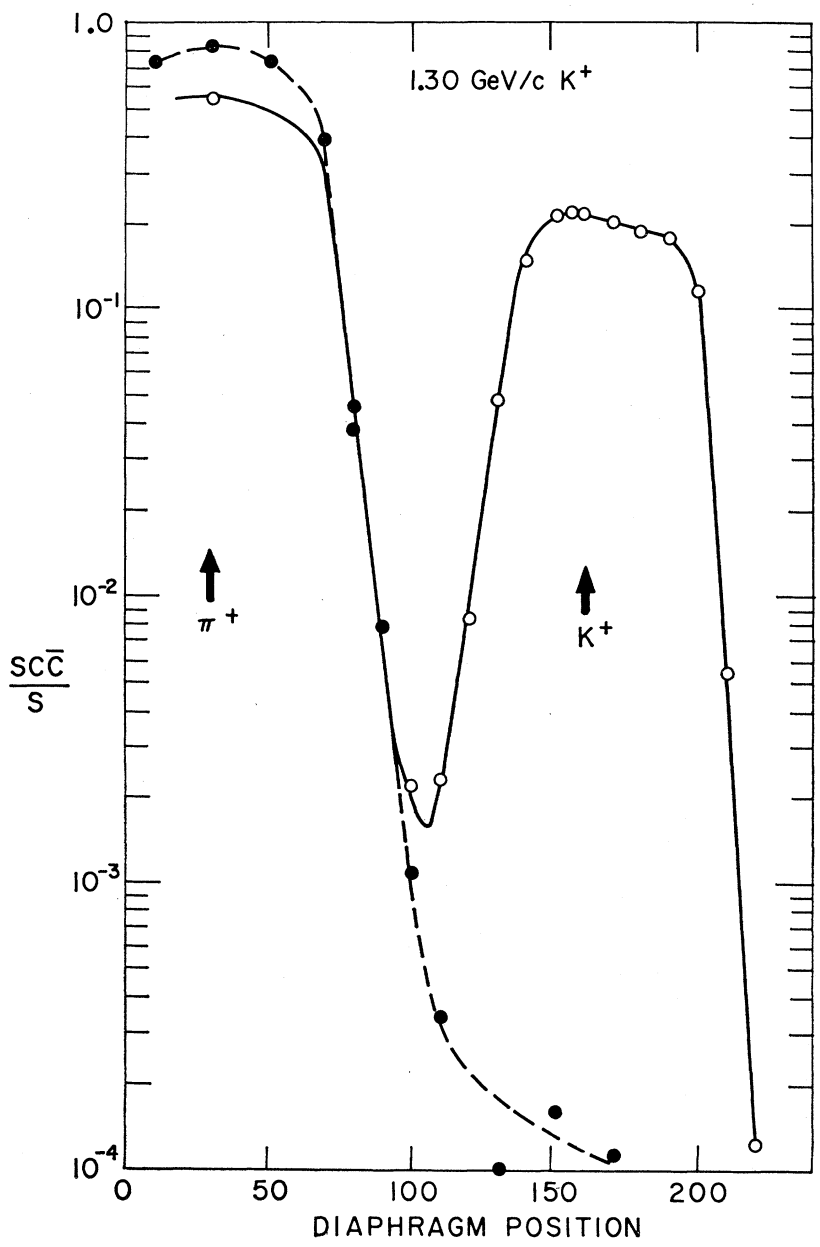

FIG. 5. Čerenkov-counter β curves. Solid curve is obtained when the separated beam is tuned to kaons, dashed curve when the beam is tuned to pions.

The target length of 93.3 cm was chosen as a compromise between the requirements of high counting rates, low multiple scattering, and good resolution. Target lengths were determined to better than 0.2%; they were measured at room temperature and corrected for thermal contraction. Transverse target dimensions were considerably larger than beam size; therefore, the alignment of the targets was not critical. The hydrogen, deuterium, and dummy targets were mounted side by side on a frame which rolled on rails, so that each target could easily be positioned on the beam line. A carbon target, made of two identical pieces which could be fastened to the two extremes of the dummy target, was also used. Table II summarizes the most important properties of the targets.

IV. EXPERIMENTAL PROCEDURE

For each type of particle, total cross-section measurements were made at approximately 50-MeV/c intervals, with monotonically increasing or decreasing momentum. Some points were measured twice as a check on reproducibility. At each momentum, the typical sequence of operation for a single measurement was

$$B\beta\epsilon EHHEDDEHHEDDCE\epsilon,$$

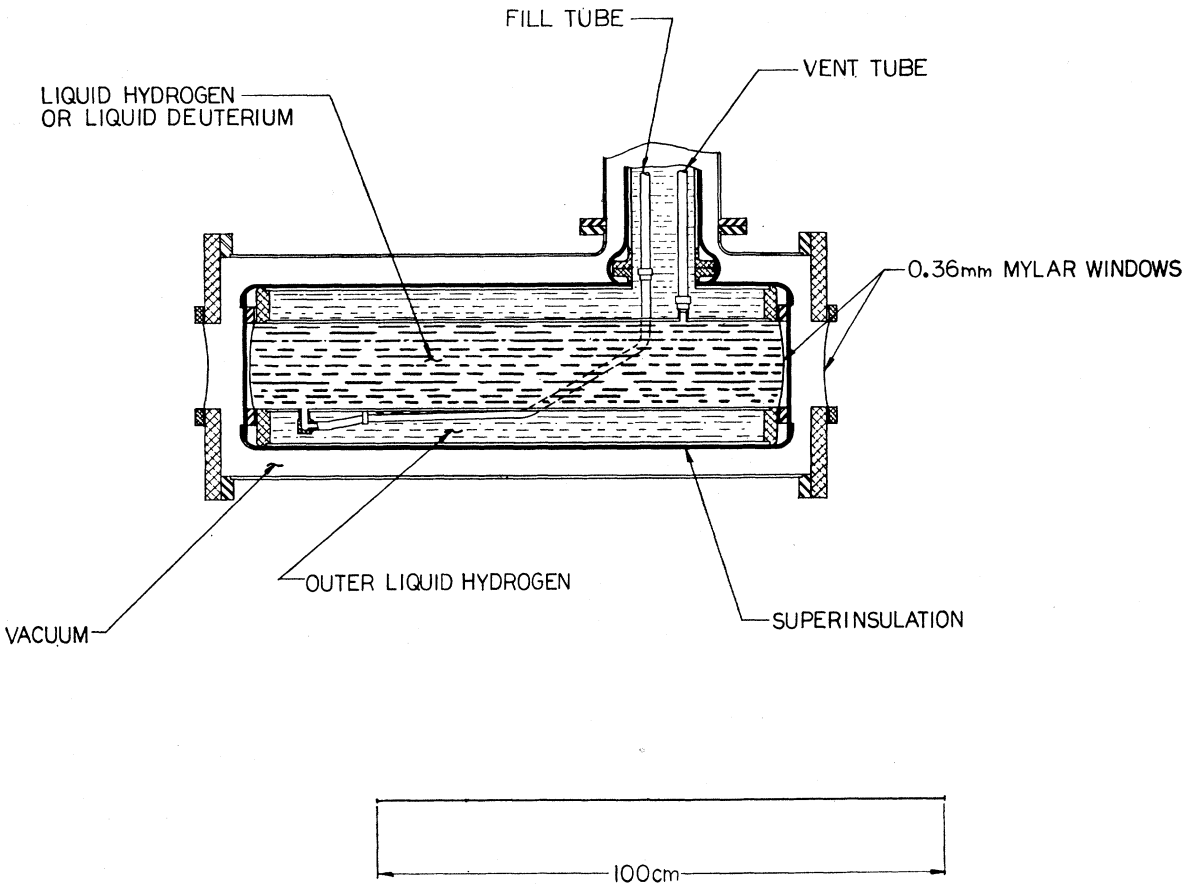

FIG. 6. Liquid-hydrogen target.

where B indicates beam tuning after a change in momentum, β indicates the running of β curves with the Čerenkov counter, ϵ indicates an efficiency check of the transmission counters, and E, H, D, and C correspond to runs with empty (dummy), hydrogen, deuterium, and carbon targets, respectively. The carbon data were used mainly as a monitor for possible structure introduced by instrumental effects, since any real structure should be smeared out by the Fermi motion in the carbon nucleus. No such structure was observed, and since no attempt was made to obtain a good geometry for the carbon measurement, these data are not included in the present paper.

Beam tuning was performed by changing the magnet currents to the computed values and then peaking the K-meson intensity and/or the K-to-π ratio with the beam elements D_2, separator 1, Q_3, and Q_6, in that order. An iteration procedure was sometimes necessary. Two β curves of the type shown in Fig. 5 were then taken to check the efficiency of the Čerenkov counter, and the K-to-π ratio in the beam before and after the electronics separation with the Čerenkov counter. At each momentum it was required that the π-meson contamination in the incident K-meson coincidence signal be below 0.1%. The efficiency ϵ of the transmission counters was measured by observing what

TABLE II. Average pressure, temperature, density, and length of targets used. Target length is given in cm, g cm^{-2}, and as the momentum lost in the target by 1.5-GeV/c kaons.

Target material	Vapor pressure (psi)	Temp. (°K)	Density (g cm^{-3})	Target length (cm)	Target length (g cm^{-2})	Target length at 1.5 GeV/c (MeV/c)
Hydrogen	18.0	20.97	0.0700±0.0001	93.4 ±0.2	6.535±0.022	28.4
Deuterium	8.3	20.97[a]	0.1690±0.0005	93.2 ±0.2	15.75 ±0.06	34.4
Carbon	···		1.694 ±0.006	6.35±0.02	10.77 ±0.04	21.2

[a] The temperature of the deuterium was taken to be the same as the temperature of the hydrogen in the outer jacket of the target.

percentage of the K mesons, which were detected in S_{11}, was also detected in the transmission counters S_i. It was required that $(S_iKS_{11})/(KS_{11})$ be at all times greater than 99.8% for each of the transmission counters. Every empty and full run was made with typically two million incoming K mesons (four million for the π mesons). The sequence used allows a check of fluctuations by comparing different runs.

After each run the readings of the scalers were printed out and also punched on paper tape. The data on paper tape were subsequently converted to IBM cards and processed by means of an IBM 7094 and subsequently a CDC 6600 computer. The computer was programmed to compute for each transmission counter the partial cross section σ_i, its statistical error, and the consistency of data from the different runs. σ_i was corrected for the difference in decay in flight between the empty and the full targets. Linear extrapolation to zero solid angle was performed by hand on a large-scale graph to give preliminary values for the total cross sections.

Total beam intensity in the telescope was never allowed to exceed 120 000 particles per machine burst in order to avoid pile-up effects and random effects. To satisfy this condition, at the higher energies the K-meson beam intensity was reduced. For pions, however, a beam shutter had to be used. Beam spill was continuously displayed on an oscilloscope. It was typically 300–400 msec long without major structure. A structure, which was sometimes present at the end of beam spill, was usually gated off. Fluctuations due to the electronic circuits were minimized by the use of relatively small beam fluxes and by air-conditioning and temperature-stabilizing to ±1°C the trailer in which they were contained.

V. DATA ANALYSIS

This experiment was performed to search for energy-dependent structure in the total cross sections. Great care was therefore exercised in order to avoid relative energy-dependent errors greater than ±(0.1–0.2)%. No particular precautions were taken to obtain an absolute cross-section accuracy to much better than about ±1%. It was necessary to apply several corrections to the data in order to obtain this absolute accuracy. Typical values of the largest of these corrections are listed in Table III. All of the corrections are slowly varying functions of energy and are therefore not expected to alter significantly the shapes of the curves of cross section versus momentum.

TABLE III. Typical values of corrections to the total cross sections. Within the quoted accuracy, the dummy target corrections, the decay corrections, and the single Coulomb scattering corrections are the same for both hydrogen and deuterium.

Laboratory momentum (GeV/c)	Corrections to data (mb) Dummy target	Decay	Single Coulomb	Coulomb-nuclear interference For hydrogen	For deuterium	Deuteron screening term (mb)
			K^- mesons			
1.0	−0.74	−2.74	−0.13	−0.12	−0.13	4.69
1.5	−0.60	−1.08	−0.05	−0.03	−0.03	2.36
2.0	−0.54	−0.59	−0.03	+0.03	+0.03	1.99
2.4	−0.49	−0.41	−0.01	+0.04	+0.04	1.86
			K^+ mesons			
1.0	−0.44	−2.74	−0.13	−0.31	−0.34	0.79
1.5	−0.45	−1.08	−0.05	−0.32	−0.40	0.83
2.0	−0.42	−0.59	−0.03	−0.24	−0.30	0.79
2.4	−0.40	−0.41	−0.01	−0.20	−0.25	0.76

A. Empty-Target Correction

One correction arose because the dummy target was not exactly equal to the empty hydrogen and deuterium targets. The main differences were that no superinsulation was included on the end windows of the dummy, and it was not evacuated. The correction for this effect was both computed and measured by comparing the dummy target rate with the empty hydrogen target rate at 1.8 GeV/c. The corrections for other momenta, shown in Table III, were then obtained by scaling the correction for 1.8 GeV/c proportionally with the carbon cross sections.

B. Deuteron Target Contamination

The deuterium used in the experiment contained a hydrogen contamination in the form of HD molecules. Assays indicated that the extent of this contamination was only 0.6 mole %. This was taken into account and resulted in a correction of +0.15% to the deuterium total cross sections. The hydrogen had essentially no contamination.

C. Decay Correction

A third correction arises from the difference in momentum loss between the dummy and full targets (see Table II) and as a consequence different decay probabilities. The correction $\Delta\sigma$ in the cross section due to this effect is given in first approximation by

$$\Delta\sigma = -\frac{m}{N l_1 \rho_t \tau c}\left(\tfrac{1}{2}l_1 + l_2\right)\frac{\Delta p}{p_0{}^2}, \qquad (4)$$

where m and τ are mass and lifetime at rest of the decaying particle, N is Avogadro's number, l_1 and ρ_t are the length and density of the target, respectively, c is the speed of light, l_2 is the distance from the back of the target to the transmission counters, p_0 is the incoming momentum, and Δp is the momentum loss in the target.

Formula (4) does not take into account the possibility that a decay particle may hit one or more transmission counters. This effect was investigated by means of a Monte Carlo program applied to the $K_{\mu 2}$ and $K_{\pi 2}$ decays only. The result is a decrease of the decay

correction by less than 5% at 1.5 GeV/c, and so it was ignored. Typical values of the decay correction are shown in Table III. It is essentially negligible for π mesons.

D. Accidental and Dead-Time Effects

Accidental coincidences between K mesons and other particles in the beam were reduced by one or two orders of magnitude due to the separated beam. Protons and antiprotons were eliminated from the beam altogether by the two electrostatic separators. Because the internal target consisted of a Be wire 0.050 in. in diameter, photon conversion to electron pairs in the target was minimized; as a result, electron contamination in the beam was very low. This was important for the measurement of π-meson total cross sections; electrons were eliminated by the separators when they were tuned to K mesons. In the measurement of K-meson total cross sections, the particles that could contribute to chance accidentals are muons and π mesons which were not removed by the separators. Both types of particles are eliminated electronically by the differential Čerenkov-counter anticoincidence $\bar{C}$. The only source of accidentals left was that in which two K mesons come through within the resolving time of the electronics, and this turned out to be negligible.

The coincidence signal S ($S_1S_2S_3\bar{G}$) was set to ignore a beam particle if it was preceded by another beam particle within 100 nsec, in order to eliminate scaler dead-time effects.

E. Extrapolation to Zero Solid Angle

A linear extrapolation to zero solid angle as determined by formula (3) was performed by hand on a large-scale graph. This procedure turned out to be the most convenient one, since it allowed an easy detection of the counters not affected by multiple scattering and also a further check on the general consistency of the data. The final error was estimated on the basis of the individual errors on each partial cross section σ_i, as well as on the goodness of the extrapolation line. At the highest energies a correction had to be applied to the total cross sections obtained by linear extrapolation, since the partial cross sections began to show a definite curvature. The correction was a smooth one, increasing for K^- mesons from zero at 1.7 GeV/c to +0.6% on hydrogen and +0.9% for deuterium at 2.45 GeV/c. The correction was about half as large for K^+ mesons.

F. Single Coulomb Scattering

The cross section σ_i as observed with the ith transmission counter corresponds not only to nuclear processes but also to single Coulomb scattering and to scattering arising from the interference of the real part of the nuclear amplitude with the Coulomb amplitude:

$$\sigma_i=\int_{-\infty}^{t_i}|f_N+f_C|^2dt+\sigma_{i\,(\mathrm{inel})}$$

$$=\int_{-\infty}^{t_i}(|f_N|^2+|f_C|^2+2f_C\,\mathrm{Re}f_N)dt+\sigma_{i\,(\mathrm{inel})}, \quad (5)$$

where f_N and f_C are the nuclear and Coulomb elastic scattering amplitudes; f_C is essentially real. $|f_C|^2$ gives rise to single Coulomb scattering and $2f_C\,\mathrm{Re}f_N$ to Coulomb-nuclear interference. t is the four-momentum transfer squared; t_i is the momentum transfer corresponding to the maximum scattering angle detected by the ith transmission counter.

The single Coulomb scattering contribution may be written as

$$(\Delta\sigma_i)_C=\int_{-\infty}^{t_i}|f_C|^2dt=\mathcal{C}^2\int_{-\infty}^{t_i}[S_p(t)]^2\frac{dt}{t^2}$$

$$=\mathcal{C}^2[2c_p\,\mathrm{Ei}(2c_pt_i)-e^{2c_pt_i}/t_i], \quad (6)$$

where $\mathcal{C}^2=5.12\times10^{-16}$ GeV cm/c is the constant for Rutherford scattering. $S_p(t)$ is the proton charge form factor for which we used the exponential form $S_p(t)=e^{c_pt}$, with $c_p=2.3$ (GeV/c)$^{-2}$.[6] $\mathrm{Ei}(2c_pt_i)$ is the exponential integral function. The data were corrected for this effect by computing the contribution for each transmission counter used in the extrapolations from (6), extrapolating the contribution to zero solid angle in the same manner as the data, and subtracting these extrapolated values from the data. Typical values for the correction are listed in Table III.

G. Coulomb-Nuclear Interference

The Coulomb-nuclear (CN) interference contribution to scattering from protons may be written as

$$(\Delta\sigma_i)_{\mathrm{CN}}=2\int_{-\infty}^{t_i}f_C\,\mathrm{Re}f_Ndt$$

$$=\pm2\mathcal{C}\int_{-\infty}^{t_i}\frac{S_p(t)\,\mathrm{Re}f_N(t)}{t}dt. \quad (7)$$

The positive (negative) sign is for a positive (negative) incident beam. For the t dependence of the real part of the nuclear amplitude, the exponential form was taken from elastic scattering, $\mathrm{Re}f_N(t)=\rho[\mathrm{Im}f_N(0)]e^{\frac{1}{2}bt}$, where ρ represents the ratio of the forward real part to the forward imaginary part of the kaon-nucleon scattering amplitude. The forward imaginary part was determined from the (uncorrected) measured total cross sections σ_T by the optical theorem. With these

[6] R. Hofstadter, F. Bumiller, and M. Croissiaux, Phys. Rev. Letters 5, 263 (1960).

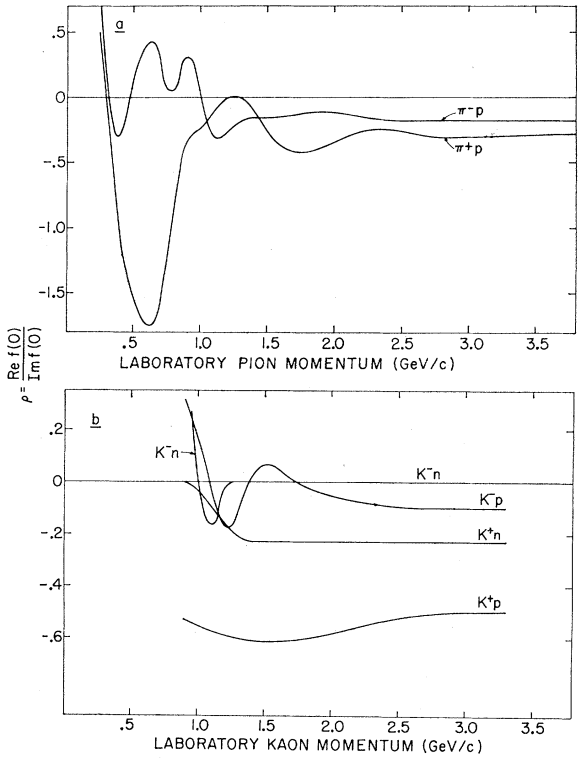

FIG. 7. Values for the ratio of real to imaginary part of the forward scattering amplitudes used for computing corrections to the total cross sections. They were taken from the dispersion-relations calculations of Ref. 10 for $\pi^{\pm}$-p and Ref. 11 for $K^{\pm}$-p and $K^{\pm}$-n.

approximations, (7) can be integrated to give

$$(\Delta\sigma_i)_{\mathrm{CN}}=\pm\alpha\rho\sigma_T\,\mathrm{Ei}[(\tfrac{1}{2}b+c_p)t_i]. \quad (8)$$

The slopes b of the differential elastic cross sections have been taken from the literature: $b_{K^+p}=4.0$,[7,8] $b_{K^-p}=7.7$,[7,9] $b_{\pi^-p}=9.0$,[1] and $b_{\pi^+p}=9.0$[1] $(\mathrm{GeV}/c)^{-2}$. α is the fine-structure constant. The ratios ρ of the real-to-imaginary forward scattering amplitudes were taken from dispersion-relation evaluations.[10,11] They are shown in Fig. 7.

The situation is more complicated for the CN interference in deuterium. We have taken into account not only elastic scattering but also deuteron breakup by using the expression

$$\left(\frac{d\sigma}{dt}\right)_{d\to d,\to pn}=|f_p|^2+|f_n|^2+2[\mathrm{Re}(f_p{}^*f_n)]S_d(t), \quad (9)$$

where f_p and f_n are the scattering amplitudes for free protons and neutrons. $S_d(t)$ is the deuteron form factor.

By writing $f_p=f_{pN}+f_{pC}$, i.e., as a sum of nuclear and Coulomb terms, and $f_n=f_{nN}$ only, one has

$$\left(\frac{d\sigma}{dt}\right)_{d\to d,\to pn}=(|f_{pN}|^2+|f_{nN}|^2+2\,\mathrm{Re}f_{pN}{}^*f_{nN})$$
$$+|f_{pC}|^2+2f_{pC}[\mathrm{Re}f_{pN}+S_d(t)\,\mathrm{Re}f_{nN}]. \quad (10)$$

The first term of (10) represents nuclear scattering, the second term represents Coulomb scattering from a free proton, and the third term is the CN interference term which may then be expressed as

$$\left(\frac{d\sigma}{dt}\right)_{\mathrm{CN}}=\pm2\alpha(e^{c_pt}/t)(\rho_p\sigma_pe^{\frac{1}{2}b_pt}+\rho_n\sigma_ne^{(\frac{1}{2}b_n+c_d)t}), \quad (11)$$

where the subscripts p, n, and d refer to proton, neutron, and deuteron. The deuteron form factor is approximated with an exponential function with $c_p+c_d=8.4$.[12] Measurements taken in a deuterium bubble chamber indicate that the diffraction scattering on neutrons is approximately the same as on protons, i.e., $b_n=b_p$,[13] and for the accuracy desired it is sufficient to make the approximation $\sigma_p=\sigma_n=\frac{1}{2}\sigma_d$. The integration of (11) proceeds then as for Eq. (7). These corrections were applied to the data in the same manner as the single Coulomb corrections; typical values are shown in Table III.

H. Total Systematic Uncertainty

Since the main objective of this experiment was to search for structure in the cross sections, no great care was exercised to obtain an absolute scale to better than $\pm1\%$. The systematic uncertainty in the absolute cross-section values arises mainly from the extrapolation procedure ($\pm0.5\%$), the CN interference correction ($\pm0.3\%$) for K^+ and ($\pm0.1\%$) for K^-, the knowledge of the target length ($\pm0.2\%$), and, in the case of deuterium, from the knowledge of the target density and target contamination ($\pm0.2\%$). A more detailed discussion of the uncertainty in the absolute scale can be found in Ref. 14.

[7] K. J. Foley, S. J. Lindenbaum, W. A. Love, S. Ozaki, J. J. Russell, and L. C. L. Yuan, Phys. Rev. Letters 11, 503 (1963).
[8] D. R. O. Morrison, in Proceedings of the Stony Brook Conference on High-Energy Two-Body Reactions, 1966 (unpublished).
[9] M. Ferro-Luzzi, in *Proceedings of the Thirteenth International Conference on High-Energy Physics, Berkeley, 1966* (University of California Press, Berkeley, Calif., 1967).
[10] O. Guisan, University of Paris, thesis, 1964 (unpublished); A. A. Carter, University of Cambridge Report No. HEP 68-1 (unpublished).
[11] M. Lusignoli, M. Restignoli, G. Violini, and G. A. Snow, CERN Report No. Th 699, 1966 (unpublished); University of Roma Nota Interna 109, 1966 (unpublished); and private communication. The real parts of the forward scattering amplitudes given in this report are not in complete agreement with the computations of other authors; see, for example, A. A. Carter, University of Cambridge Report No. HEP 68-10 (unpublished); Phys. Rev. Letters **18**, 801 (1967).
[12] J. A. McIntyre and G. R. Burleson, Phys. Rev. **112**, 2077 (1958).
[13] SABRE collaboration K^-n elastic scattering at 3 GeV/c (private communication).
[14] R. J. Abrams, R. L. Cool, G. Giacomelli, T. F. Kycia, B. A. Leontic, K. K. Li, and D. N. Michael, following paper, Phys. Rev. D **1**, 1917 (1970); K. F. Riley (to be published).

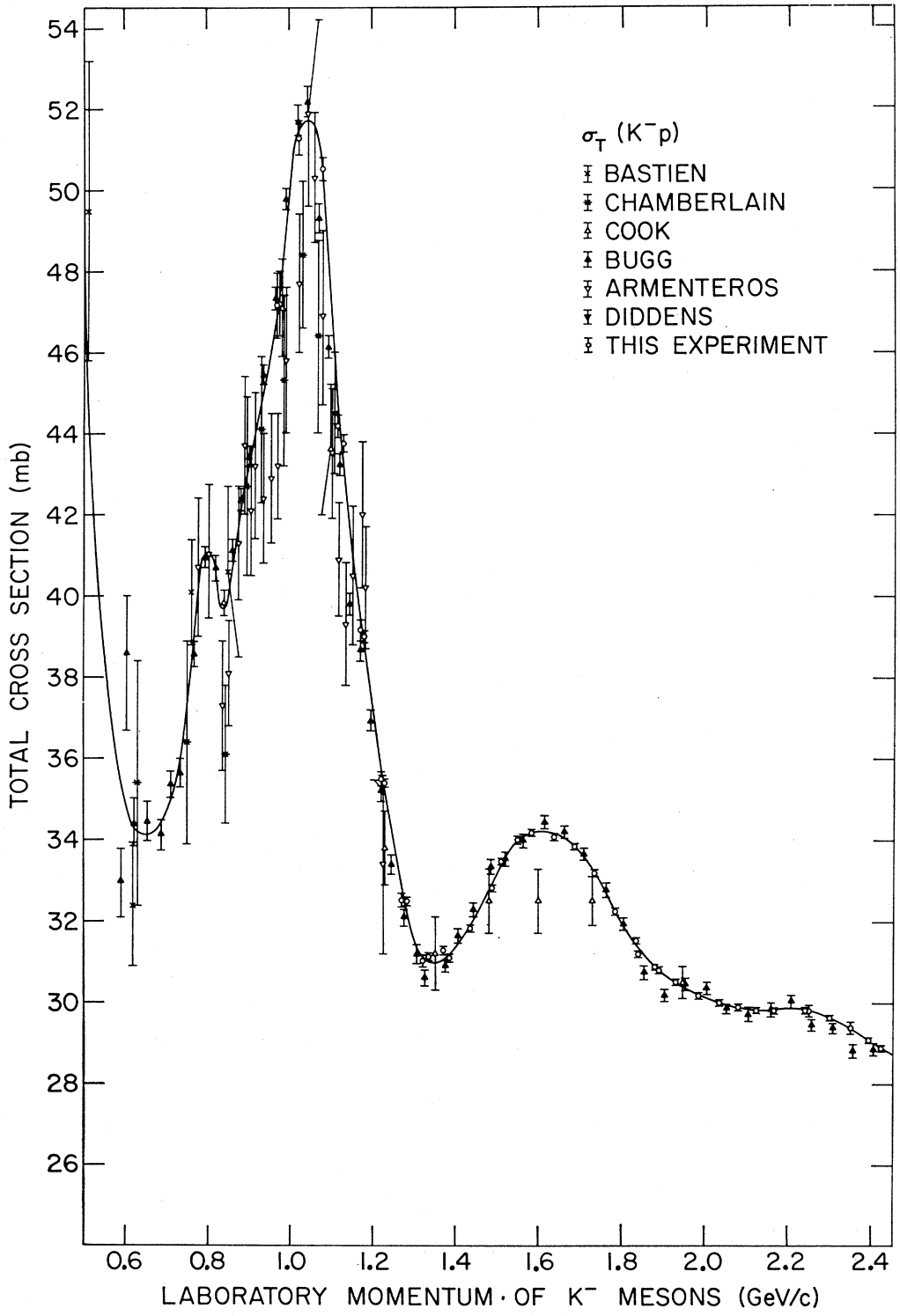

FIG. 8. K^--p total cross sections. Error bars represent point-to-point statistical standard deviations.

I. Momentum Definition and Resolution

Momentum calibration of the beam is based on the magnetic measurements of the beam transport equipment available at Brookhaven[15] and on the beam optics computation. Our reference magnet was D_3.

[15] G. T. Danby, Brookhaven National Laboratory AGS Internal Report No. GTD-2, 1961 (unpublished).

Because of the interdependence between the three bending magnets used, the absolute uncertainty in the beam momentum may be as high as 1.0%, while the relative precision between neighboring points is about 0.1–0.2%.

The experimental resolution in momentum arises from finite target length (see Table II) and finite spread in beam momentum (±1%). It amounts to about 12–15 MeV full width at half-maximum in the center-of-mass system and is almost constant with energy (slightly increasing with energy).

VI. RESULTS

The experimental results for the $K^{\pm}$-p, $K^{\pm}$-d, $\pi^{\pm}$-p, and $\pi^{\pm}$-d total cross sections are plotted in Figs. 8–12; the $K^{\pm}$-p and $K^{\pm}$-d cross sections are tabulated in Tables IV and V. All cross sections are in mb; errors represent statistical standard deviations.

TABLE IV. K^-p and K^-d total cross sections. Errors represent point-to-point statistical standard deviations. The over-all systematic error is estimated to be less than ±1%.

Laboratory momentum (GeV/c)	σ_T (K^-p) (mb)	Laboratory momentum (GeV/c)	σ_T (K^-d) (mb)
0.969	47.16±0.80	0.966	79.96±0.90
0.975	47.19±0.80	0.972	80.44±0.70
1.022	51.27±0.42	1.019	80.71±0.40
1.080	50.51±0.28	1.077	78.71±0.30
1.116	44.18±0.28	1.113	73.10±0.26
1.130	43.74±0.20	1.127	72.66±0.20
1.169	39.18±0.26	1.166	68.06±0.25
1.179	39.01±0.16	1.176	67.58±0.16
1.220	35.51±0.18	1.217	64.23±0.18
1.230	35.41±0.10	1.227	63.40±0.17
1.270	32.52±0.17	1.267	60.84±0.16
1.283	32.50±0.09	1.280	60.75±0.10
1.320	31.03±0.14	1.317	58.57±0.12
1.336	31.12±0.08	1.333	58.24±0.08
1.370	31.27±0.11	1.367	57.71±0.10
1.384	31.09±0.08	1.381	57.82±0.08
1.434	31.83±0.08	1.431	57.97±0.07
1.488	32.83±0.08	1.485	58.43±0.07
1.509	33.47±0.08	1.506	58.59±0.06
1.549	34.00±0.10	1.546	58.75±0.07
1.583	34.17±0.08	1.580	58.63±0.07
1.637	34.07±0.08	1.634	58.19±0.07
1.687	33.84±0.07	1.684	57.43±0.07
1.735	33.19±0.07	1.732	56.87±0.07
1.785	32.26±0.07	1.782	56.01±0.07
1.835	31.53±0.07	1.837	55.37±0.05
1.840	31.19±0.07	1.876	54.84±0.06
1.879	30.85±0.07	1.882	54.94±0.06
1.885	30.81±0.07	1.926	54.66±0.06
1.929	30.49±0.07	1.982	54.29±0.09
1.985	30.17±0.06	2.032	53.98±0.06
2.035	29.99±0.06	2.077	53.85±0.06
2.080	29.89±0.06	2.121	53.72±0.06
2.124	29.81±0.06	2.161	53.53±0.06
2.164	29.79±0.06	2.203	52.95±0.06
2.206	29.87±0.06	2.237	52.75±0.06
2.240	29.79±0.08	2.298	52.61±0.06
2.250	29.79±0.15	2.348	52.26±0.10
2.301	29.63±0.06	2.389	51.97±0.06
2.351	29.38±0.15	2.420	51.91±0.07
2.392	29.07±0.07		
2.423	28.88±0.07		

TABLE V. K^+p and K^+d total cross sections. Errors represent point-to-point statistical standard deviations. The over-all systematic error is estimated to be less than ±1%.

Laboratory momentum (GeV/c)	σ_T (K^+p) (mb)	Laboratory momentum (GeV/c)	σ_T (K^+d) (mb)
0.891	14.39±0.38	0.888	30.10±0.36
0.942	15.57±0.30	0.939	31.98±0.34
0.992	15.97±0.27	0.989	33.20±0.24
1.043	17.39±0.25	1.040	34.77±0.24
1.094	17.12±0.25	1.091	36.04±0.24
1.144	18.09±0.15	1.141	37.22±0.15
1.194	18.47±0.12	1.191	37.69±0.12
1.245	18.54±0.12	1.242	37.57±0.11
1.295	18.61±0.11	1.292	37.43±0.10
1.345	18.44±0.10	1.342	36.99±0.12
1.395	18.27±0.10	1.392	36.78±0.12
1.445	18.04±0.10	1.442	36.43±0.10
1.495	17.93±0.09	1.492	36.27±0.10
1.596	17.75±0.09	1.593	35.89±0.08
1.646	17.86±0.06	1.643	35.78±0.08
1.696	17.85±0.06	1.693	35.76±0.06
1.746	17.80±0.06	1.743	35.89±0.06
1.796	17.80±0.06	1.793	35.70±0.06
1.896	17.81±0.06	1.893	35.53±0.06
1.996	17.60±0.08	1.993	35.41±0.08
2.096	17.51±0.08	2.093	35.47±0.08
2.196	17.54±0.08	2.193	35.22±0.10
2.396	17.55±0.08	2.393	35.45±0.08

Figures 8–11 show our results as well as earlier published values for K^- [16–21] and K^+ [20–23] data. For the hydrogen data there is an over-all good agreement with previous results, within the stated errors. The agreement is not so good for the deuterium data but is probably compatible with the systematic uncertainties in absolute cross-section scale.

Three structures are clearly evident in the K^--p total cross-section data of Fig. 8 at laboratory momenta of 1.06, 1.66, and 2.31 GeV/c. There are also three broader and smaller structures in the K^--d total cross-section data of Fig. 9 at approximately the same momenta as that in $\sigma_T(K^-$-$p)$; the central values do not in fact correspond exactly but appear shifted to lower momenta.

One structure is clearly evident in both K^+-p and K^+-d total cross sections (Figs. 10 and 11). Again, the

[16] V. Cook, B. Cork, T. F. Koang, D. Keefe, L. T. Kerth, W. A. Wenzel, and T. F. Zipf, Phys. Rev. **123**, 320 (1961).
[17] O. Chamberlain, K. M. Crowe, D. Keefe, L. T. Kerth, A. Lemonick, Tin Maung, and T. F. Zipf, Phys. Rev. **125**, 1696 (1962).
[18] P. L. Bastien and J. P. Berge, Phys. Rev. Letters **10**, 188 (1963).
[19] R. Armenteros *et al.*, CERN Report No. DPH 2-11, 1968 (unpublished).
[20] H. C. Burrowes, D. O. Caldwell, D. H. Frisch, D. A. Hill, D. M. Ritson, and R. A. Schluter, Phys. Rev. Letters **2**, 117 (1952).
[21] D. V. Bugg, R. S. Gilmore, K. M. Knight, D. C. Salter, G. H. Stafford, E. J. N. Wilson, J. D. Davies, J. D. Dowell, P. M. Hattersley, R. J. Homer, A. W. O'Dell, A. A. Carter, R. J. Tapper, and K. F. Riley, Phys. Rev. **168**, 1466 (1968).
[22] V. Cook, D. Keefe, L. T. Kerth, P. G. Murphy, W. A. Wenzel, and T. F. Zipf, Phys. Rev. Letters **7**, 182 (1961).
[23] S. Goldhaber, W. Chinowsky, G. Goldhaber, W. Lee, T. O'Halloran, T. F. Stubbs, G. M. Pjerrou, D. H. Stork, and H. K. Ticho, Phys. Rev. Letters **9**, 135 (1962).

structures are approximately at the same momentum but, in fact, they do not correspond exactly. Moreover, the K^{+}-d structure is considerably larger than the K^{+}-p one.

The measured cross sections of $K^{\pm}$-p and $K^{\pm}$-d allow us, in principle, to deduce the cross sections for the pure $I=0$ and $I=1$ isospin states. It is well known, however, that corrections must be applied as a result of the binding of the neutron in the deuteron both for the so-called shadowing effect and for the Fermi motion of the bound nucleons. The available procedures for making such corrections are only approximations, and for this reason it would be desirable to subject them to experimental verification under similar circumstances. The pion-nucleon system affords such an opportunity. The $I=\frac{1}{2}$ and $I=\frac{3}{2}$ cross sections can be deduced directly from $\sigma(\pi^{+}$-$p)$ and $\sigma(\pi^{-}$-$p)$ without complications from the deuteron and can be compared to those deduced from $\sigma(\pi^{-}$-$p)$ and $\sigma(\pi^{-}$-$d)$ utilizing the available correction procedures. For this reason, measurements were taken of the total cross sections of $\pi^{\pm}$ mesons on protons and deuterons in the momentum range 0.90–2.45 GeV/c. The muon contamination of the beam could be deduced from the normalization of

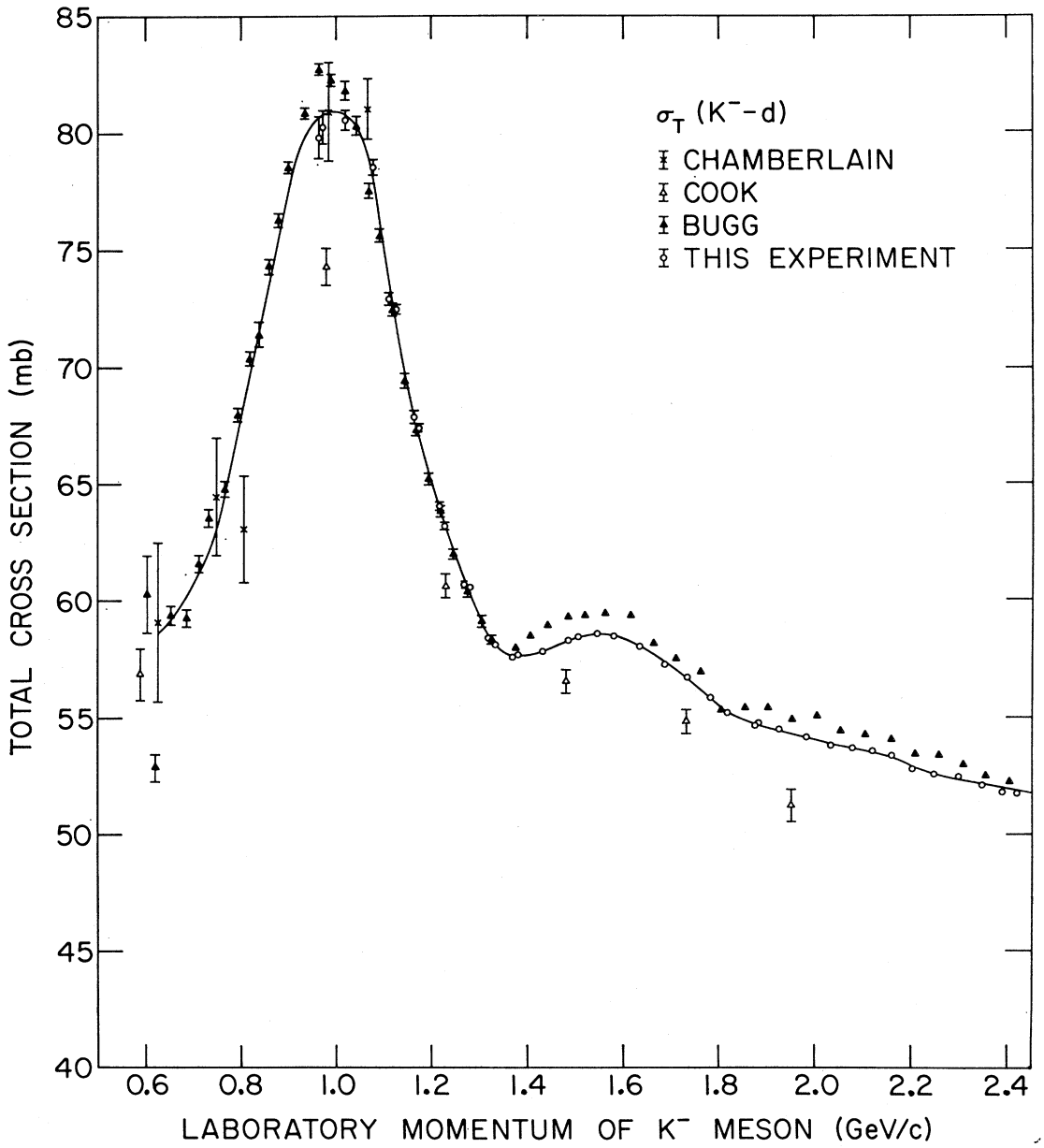

FIG. 9. K^{-}-d total cross sections. Wherever error bars are omitted, the statistical error is smaller than the size of the data point.

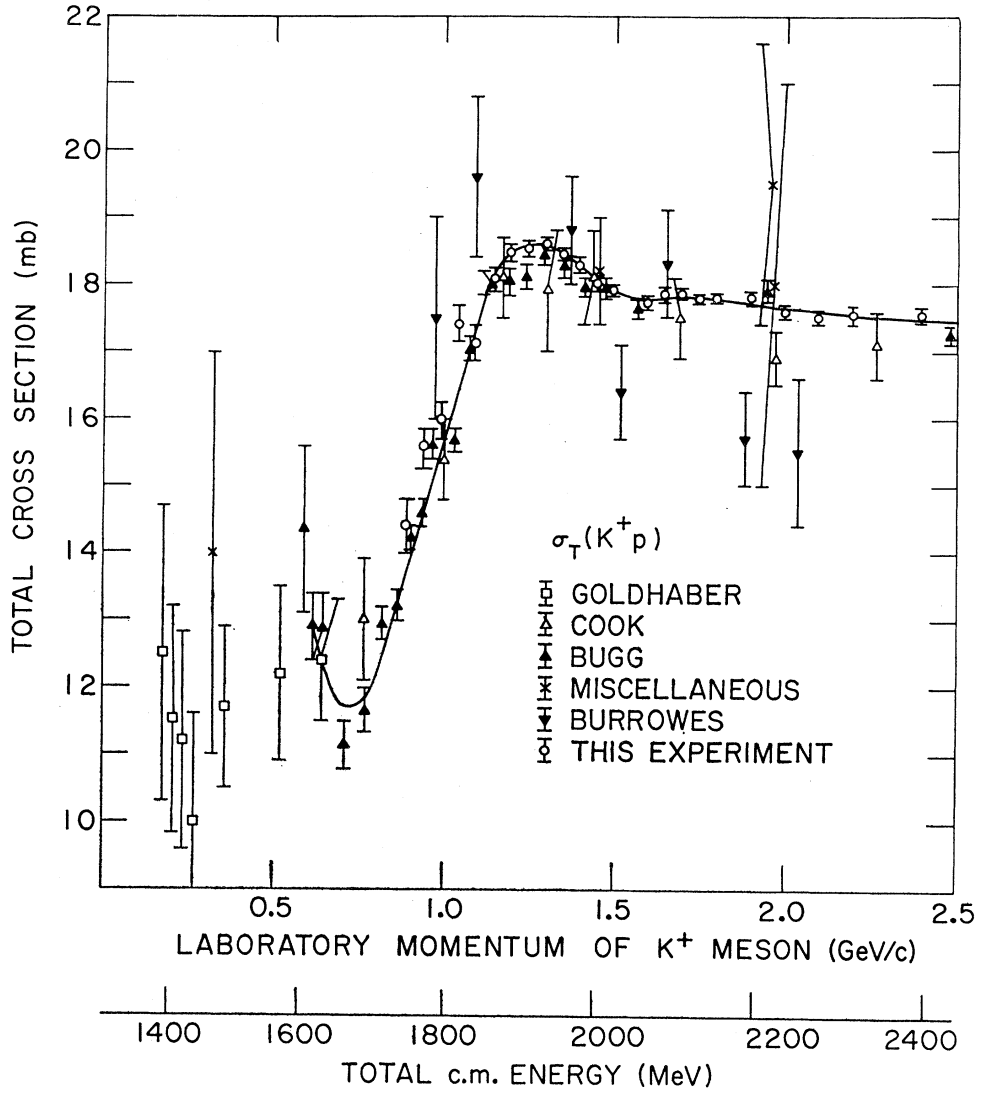

FIG. 10. K^+-p total cross sections.

the measured total cross sections to the world data[1] and assuming that $\sigma_{\pi^+d}=\sigma_{\pi^-d}$ from charge symmetry. Therefore, the total systematic uncertainty for π-meson cross sections is of the order of ± 1 to $\pm 2\%$; the point-to-point uncertainty is the same as for the K mesons for energies larger than 1.7 GeV/c. It becomes larger below 1.7 GeV/c.

The π-meson data (Fig. 12) exhibit all the well-known structures.[1] The deuteron cross section has the same peaks as the hydrogen cross sections. Within the precision of the experiment, the deuteron peaks appear at the same momentum as those in hydrogen but are somewhat broader, as is expected from the effects of the Fermi motion.

VII. COMPUTATION OF PURE ISOTOPIC-SPIN CROSS SECTIONS

The extraction of the free-neutron data from deuteron and hydrogen data is rather complicated and, as yet, a little arbitrary. We first describe our method of analysis and then apply it to the π-meson data where the correct answer is known. An estimate is thus obtained of the errors involved in the subsequent treatment of the K^- and K^+ meson results.

It has been shown[24–26] that, if the π-meson–nucleon cross sections are reasonably smooth, then the deuteron

[24] R. J. Glauber, Phys. Rev. **100**, 242 (1955).
[25] R. J. Glauber and V. Franco, Phys. Rev. **142**, 1195 (1966).
[26] C. Wilkin, Phys. Rev. Letters **17**, 561 (1966).

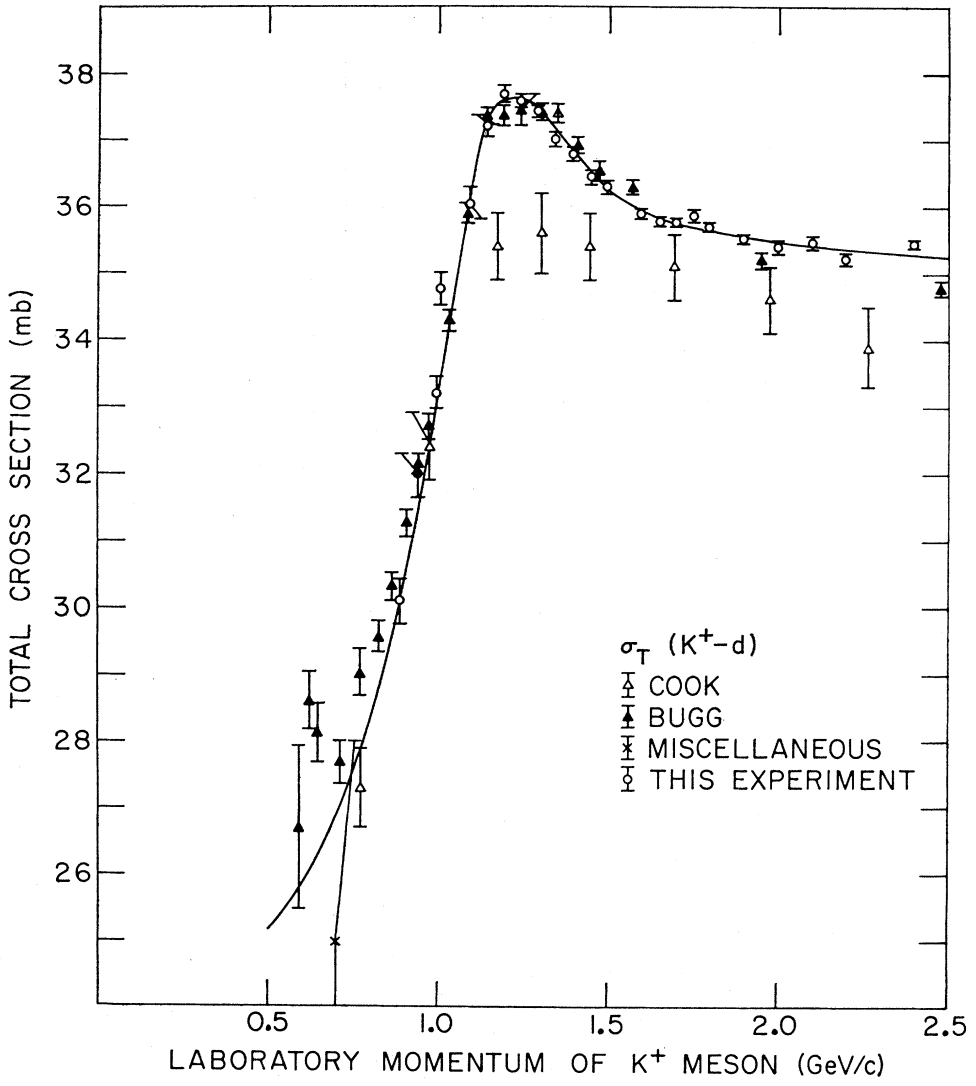

FIG. 11. K^{+}-d total cross sections.

cross section may be approximated by

$$\sigma_{\pi^+d}(p)=\sigma_{\pi^+p}(p)+\sigma_{\pi^+n}(p)-\delta\sigma\,, \tag{12}$$

where p is the laboratory momentum and the cross-section defect is

$$\delta\sigma=\frac{\langle r^{-2}\rangle}{4\pi}\{\tfrac{3}{2}\sigma_{\pi^+p}(p)\sigma_{\pi^+n}(p)[1-\rho_+\rho_-]$$
$$-\tfrac{1}{4}[\sigma_{\pi^+p}{}^2(p)(1-\rho_+{}^2)+\sigma_{\pi^-p}{}^2(p)(1-\rho_-{}^2)]\}\,, \tag{13}$$

where ρ_+ (ρ_-) is the ratio of the real-to-imaginary part of the forward scattering amplitude in π^+p ($\pi^+n=\pi^-p$) scattering. The parameter $\langle r^{-2}\rangle$ represents the average inverse square separation of points in the proton and neutron. If the effective sizes of these nucleons are small compared with the deuteron size, then this parameter will be a universal constant obtainable from nuclear physics. In practice, this will not be the case and $\langle r^{-2}\rangle$ will depend somewhat upon the nucleon size. In order to make the use of formula (12) simple, we shall assume that this size is constant, independent of the nature of the incident particle or its momentum, so that $\langle r^{-2}\rangle$ is a calculable constant or one that can be taken from experiment. Of course, for pions we could do much better than this and also take spin dependence into account, but this would be of very little help for the K mesons which are the primary interest of this paper.

The above description has to be modified if the cross sections are rapidly varying. Near a sharp resonance, the Fermi motion of the nucleons inside the deuteron spreads the peak by an amount which depends upon the mass and width of the resonance as well as the characteristics of the deuteron. The kinematics of the

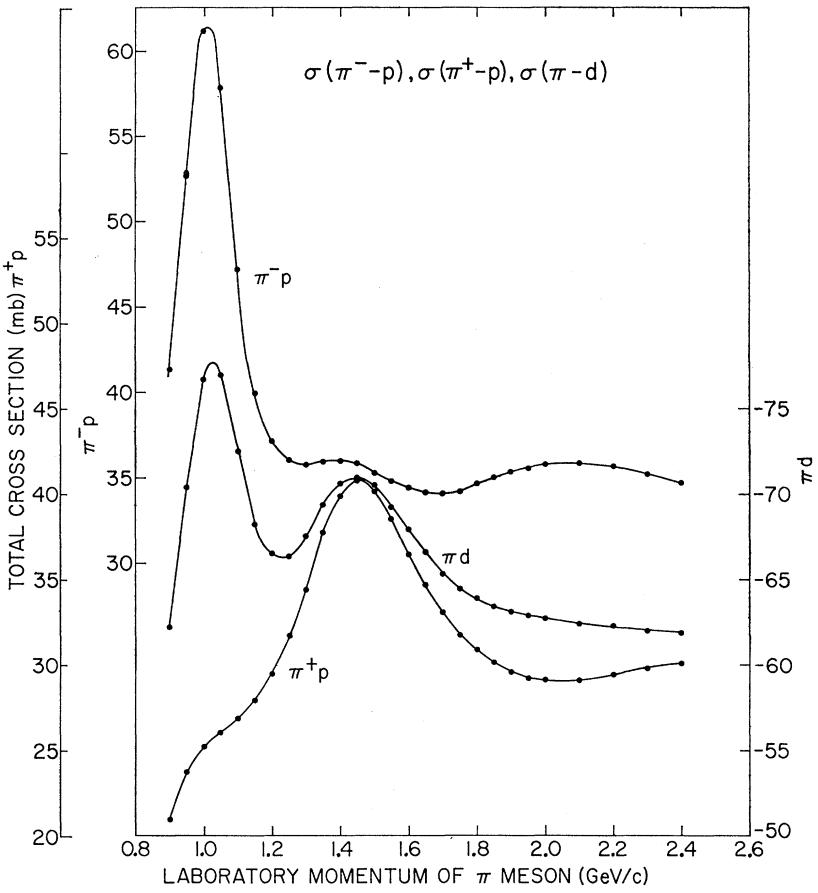

FIG. 12. π^--p, π^+-d, and π^--d total cross sections. For all points shown, statistical errors are smaller than the size of the data points.

scattering on the proton bound in the deuteron are described in Fig. 13. The deuteron at rest dissociates into a neutron of momentum $\mathbf{q}$ and a virtual proton which interacts with the incoming π^+ to form a final state of effective mass squared s_a. Since the neutron is on its mass shell (in principle, it is observable), the proton is off its mass shell. The proton cross section smeared out over the Fermi motion is then

$$\text{“}\sigma_{\pi^+p}(p)\text{”} = \int |\varphi(q)|^2 d^3q\, \sigma_{\pi^+p}(p'), \qquad (14)$$

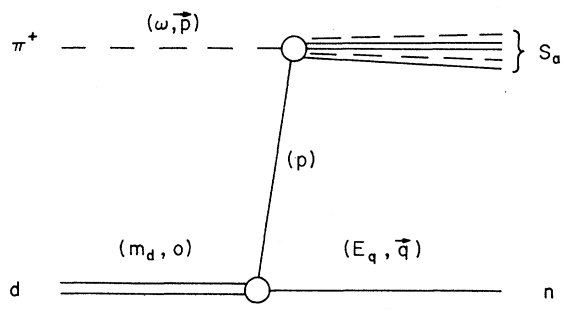

FIG. 13. Kinematics of π^+-p scattering off the proton inside the deuteron.

where p' is the laboratory momentum associated with physical π^+p scattering at a center-of-mass energy squared s_a, and $\varphi(q)$ is the normalized deuteron wave function in momentum space. It might be argued that it is more proper to smear out the relativistically invariant amplitude in (14) rather than the total cross section. However, if the correct relativistic normalization is then used, the result differs negligibly from (14) at the energy range of interest here.

We thus modify Eq. (12) by replacing the first two terms by “σ_{π^+p}” and “σ_{π^+n}”. The cross-section defect is much more complicated and, in general, the smearing would involve a five-dimensional integral. However, since $\delta\sigma$ is only a small correction and since the value of $\delta\sigma$ calculated with “$\sigma_{\pi p}$” rather than $\sigma_{\pi p}$ is quite small, our prescription is to replace $\sigma_{\pi p}$ by “$\sigma_{\pi p}$” throughout Eqs. (12) and (13).

As a first test of this procedure, we feed in the values of σ and ρ from the pion data and calculate the value of $\langle r^{-2}\rangle$ as a function of momentum. The deuteron wave function used was the S-wave part of that due to Moravcsik,[27] which fits quite well the low-energy np

[27] M. Moravcsik, Nucl. Phys. **7**, 113 (1958).

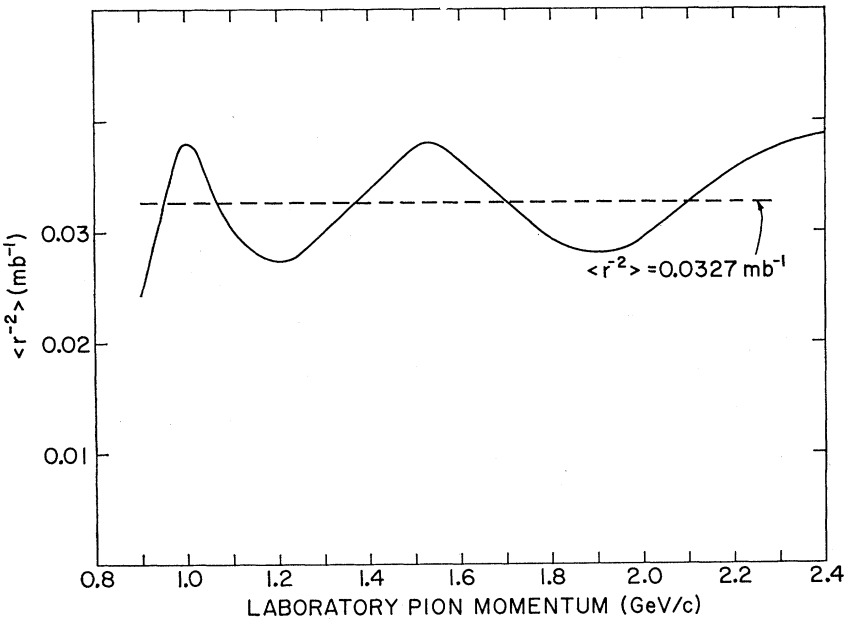

FIG. 14. $\langle r^{-2}\rangle$, the average value of the inverse of the square of the neutron-proton separation in the deuteron, computed from t e pion data.

data:

$$\psi(r)=C(e^{-\alpha r}-e^{-\beta r})(1-e^{-\gamma r})(1-e^{-\delta r})/r, \quad (15)$$

where $\alpha=0.232$ F^{-1}, $\beta=1.90$ F^{-1}, $\gamma=1.59$ F^{-1}, and $\delta=2.5$ F^{-1}; C is the normalization constant. If the preceding analysis is right, then $\langle r^{-2}\rangle$ should be a constant, independent of momentum. From the graph of the results in Fig. 14, it can be seen that $\langle r^{-2}\rangle$ fluctuates about a mean $\langle r^{-2}\rangle=0.0327$ mb^{-1} with a variation equal to ± 0.0037 mb^{-1}. The mean value is in good agreement with that obtained with point nucleons using the wave function (15), viz., $\langle r^{-2}\rangle=0.03$ mb^{-1}, although the low-energy data are not very sensitive to the quantity. The peaks and valleys of $\langle r^{-2}\rangle$ are in rough correspondence with those of $\sigma_{\pi d}$, which perhaps indicates that the wave function should be modified to smear the cross sections more. This has been tried, but only a small portion of the curve can be so smoothed out and the variation is not reduced much.

Carter *et al.*[28] found similar results between 0.9 and 2.45 GeV/c. In the treatment of their K-meson data, Bugg *et al.*[21] used an average value $\langle r^{-2}\rangle=0.029$ mb^{-1}. Using their data below 0.9 GeV/c and the same analysis procedure, however, they found that $\langle r^{-2}\rangle$ decreases precipitously, reaching a minimum at a negative value ($\langle r^{-2}\rangle=-0.027$ mb^{-1}) at 0.84 GeV/c. Assuming the accuracy of the experimental data, the error introduced by the approximation procedures used above are clearly larger below 0.9 GeV/c.

In another more complicated experiment by Bellettini *et al.*,[29] involving deuterons, a shift in the resonance

[28] A. A. Carter, K. F. Riley, R. J. Tapper, D. V. Bugg, R. S. Gilmore, K. M. Knight, D. C. Salter, G. H. Stafford, E. J. Wilson, J. D. Davies, J. D. Dowell, P. M. Hattersley, R. J. Homer, and A. W. O'Dell, Phys. Rev. **168**, 1457 (1968).

[29] G. Bellettini, G. Cocconi, A. N. Diddens, E. Lillethun, J. P. Scanlon, A. M. Shapiro, and A. M. Wetherell, Phys. Letters **18**, 167 (1965).

TABLE VI. K^-N total cross sections for the $I=0$ and $I=1$ isotopic spin states. Errors represent point-to-point statistical standard deviations. The over-all systematic error, including uncertainties in correcting for screening and Fermi motion in the deuteron, may be as high as $\pm 8\%$.

Laboratory momentum (GeV/c)	σ_0 (K^-N) (mb)	σ_1 (K^-N) (mb)
0.966	52.98±2.56	40.89±1.20
0.972	52.69±2.50	41.24±1.06
1.019	66.49±1.32	35.80±0.58
1.077	68.07±0.89	33.51±0.41
1.113	59.39±0.88	29.72±0.38
1.127	59.83±0.63	28.40±0.28
1.166	51.17±0.82	27.76±0.36
1.176	50.97±0.51	27.57±0.23
1.217	42.92±0.57	28.51±0.25
1.227	43.21±0.34	28.00±0.20
1.267	36.71±0.53	28.62±0.23
1.280	36.82±0.29	28.42±0.13
1.317	35.04±0.44	27.13±0.18
1.333	35.56±0.25	26.73±0.11
1.367	35.57±0.34	26.93±0.15
1.381	34.41±0.25	27.71±0.11
1.431	35.41±0.25	28.14±0.11
1.485	37.29±0.25	28.25±0.11
1.506	38.86±0.25	27.97±0.10
1.546	40.14±0.31	27.79±0.12
1.580	40.92±0.25	27.39±0.11
1.634	41.67±0.25	26.49±0.11
1.684	42.08±0.22	25.67±0.10
1.732	40.85±0.22	25.62±0.10
1.782	39.54±0.22	25.08±0.10
1.837	38.02±0.22	24.98±0.09
1.876	36.47±0.22	25.29±0.09
1.882	36.19±0.22	25.49±0.09
1.926	35.19±0.22	25.83±0.09
1.982	34.50±0.20	25.87±0.11
2.032	34.22±0.19	25.78±0.08
2.077	33.93±0.19	25.86±0.08
2.121	33.65±0.19	25.97±0.08
2.161	33.79±0.19	25.79±0.08
2.203	35.00±0.19	24.75±0.08
2.237	35.26±0.25	24.33±0.10
2.298	34.80±0.19	24.48±0.08
2.348	34.26±0.46	24.54±0.18
2.389	33.60±0.22	24.58±0.09
2.420	33.05±0.22	24.75±0.10

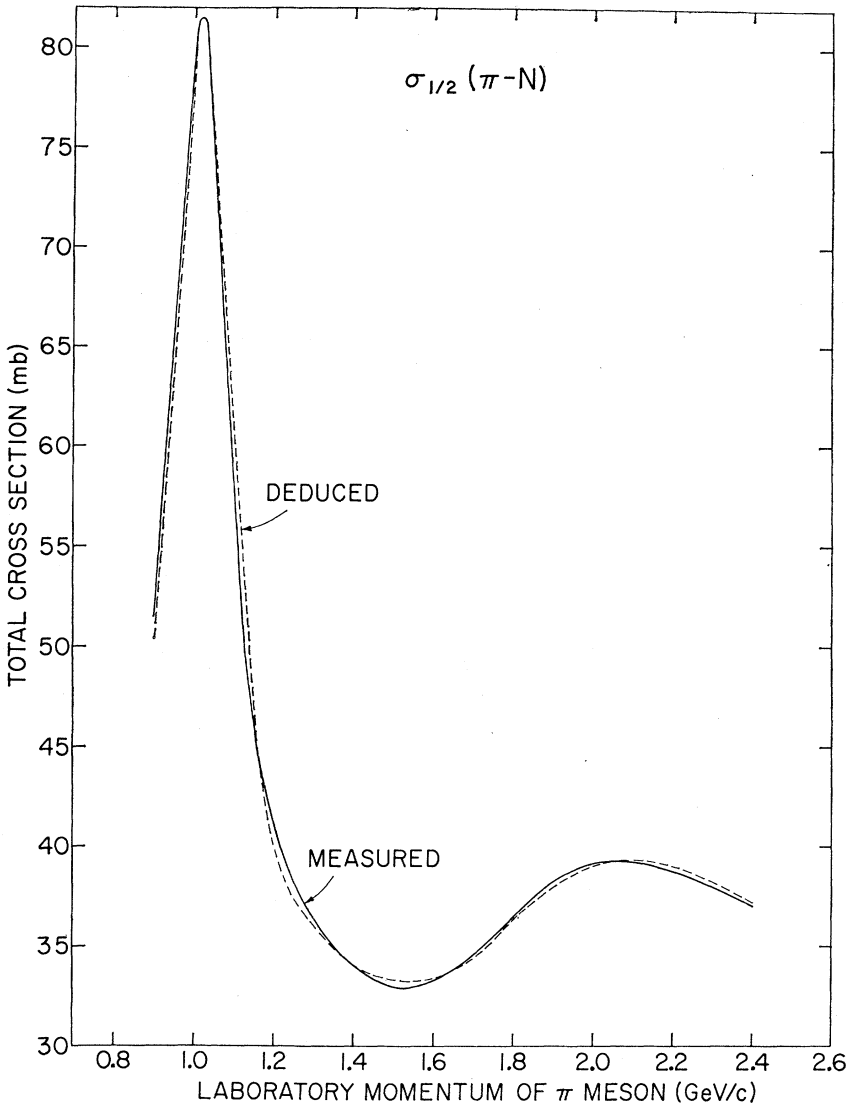

FIG. 15. $I=\frac{1}{2}$ pion-nucleon total cross section. Solid line was computed algebraically from π^--p and π^+-p data; dashed line was computed using π^--p and π^--d data, taking into account the effects of screening and Fermi motion in the deuteron.

momentum of deuterons was observed and was interpreted as being due to coherent processes in which the deuteron acts as a single scatterer. If such a shifting were present in our data, then it should show up as maxima and minima in $\langle r^{-2}\rangle$ exactly out of phase with the maxima and minima of $\sigma_{\pi d}$. We thus conclude that any shifting is almost certainly less than 10 MeV/c.

In the derivation of formula (12) and of subsequent ones, many approximations have been made and so the variation in $\langle r^{-2}\rangle$ is not too surprising. $\langle r^{-2}\rangle$ differs appreciably from its mean value mainly in regions where there is a large structure in the cross sections. Consequently, difficulties of interpretation only arise when we are looking for a small peak at a position where there is a strong maximum or minimum in the other isotopic spin state. $\langle r^{-2}\rangle$ was also calculated neglecting the real parts of the amplitudes. Neither the mean value nor the variation altered significantly.

After the application of (12) to obtain the neutron cross sections, a cross section is obtained which is averaged over the Fermi motion. Thus the problem of unfolding the Fermi motion, i.e., of inverting Eq. (14), needs to be solved next. By adding $\sigma(p)$ to both sides of Eq. (14) and rearranging, we obtain, since φ is normalized to unity,

$$\sigma(p)=\text{“}\sigma(p)\text{”}-\int|\varphi(q)|^2 d^3q\,[\sigma(p')-\sigma(p)]. \quad (16)$$

But since p' is constrained by the deuteron wave function to differ from p by a small amount, the contribution from the integral is relatively small. This is

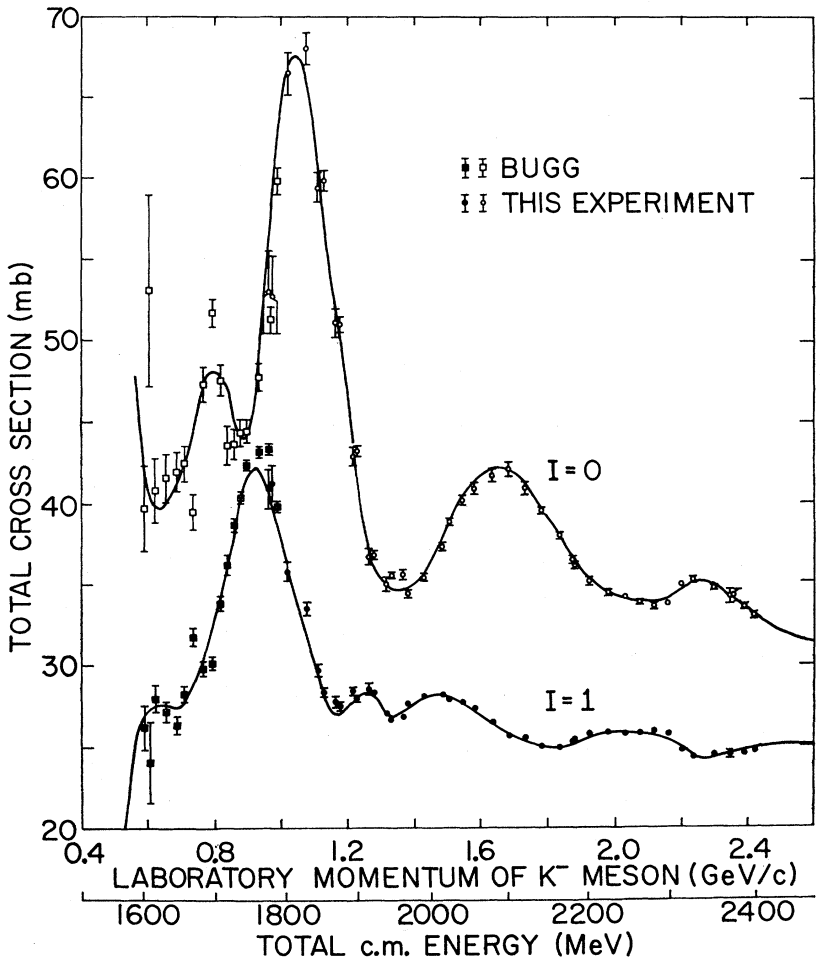

FIG. 16. Total cross sections σ_0 and σ_1 for the $I=0$ and $I=1$ isotopic spin states, respectively, for the K^--N system. Error bars represent point-to-point statistical standard deviations; if the error is smaller than the size of the dot, it is not indicated.

just an expression of the fact that the smeared and unsmeared cross sections are very similar. Equation (16) can be iterated in the form

$$\sigma_{n+1}(p)=\text{“}\sigma(p)\text{”}-\int|\varphi(q)|^2 d^3q\,[\sigma_n(p')-\sigma_n(p)]. \quad (17)$$

Suppose now that there is a very sharp resonance in the π^+p system; in the smeared data it will appear as a very small bump and so it will be unfolded by (17) only after many iterations. It is, of course, possible that the smeared bump is not statistically significant. This implies that the indiscriminate use of a large number of iterations of (17) can lead essentially to noise. A rough criterion for its use is the following. Every time (17) is iterated, it is equivalent to the differentiation of the input data. If a structure is determined by n points with no error, then in principle one can define $n-1$ derivatives and thus try the $(n-1)$th iteration. In practice, the points do have statistical fluctuations which can introduce spurious structure. We found that this effect could best be minimized by passing smooth curves through the points before the unfolding and limiting the unfolding to the third iteration.

A second and quantitative test of the validity of the above procedure may be obtained by using a constant $\langle r^{-2}\rangle$ and real parts as shown in Fig. 7, computing the $I=\frac{1}{2}$ pion-nucleon cross sections from the π^-p and π^-d data, and comparing them with that obtained algebraically from the π^-p and π^+p data. The dashed curve of Fig. 15 shows the $I=\frac{1}{2}$ cross section deduced from the deuteron data. This has to be compared with the solid curve which was computed algebraically from the following relationship:

$$\sigma_{1/2}=\tfrac{1}{2}[3\sigma(\pi^-p)-\sigma(\pi^+p)]. \quad (18)$$

The excellent agreement between the two curves gives us confidence in the application of the above deuteron analysis to the kaon data. Other deuteron wave functions were tried (Hulthén and Gaussian) with different high-momentum cutoffs. The results obtained differ little from the results using the Moravcsik wave function, but low-energy nuclear physics tells us very little about the high-momentum components of the deuteron.

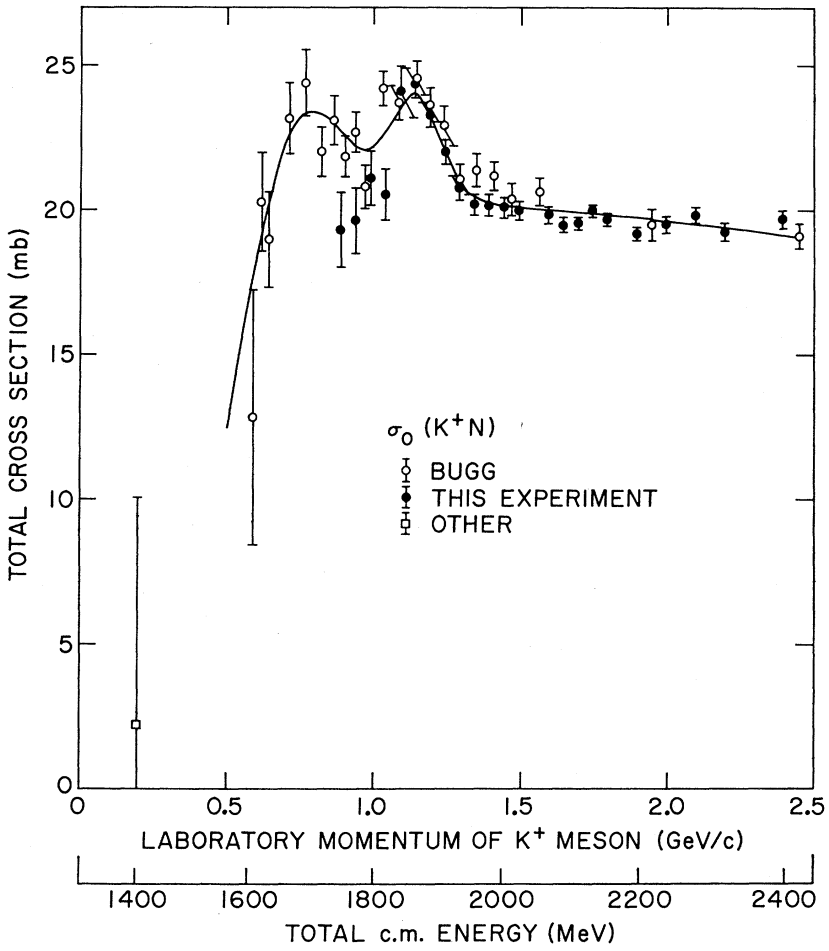

FIG. 17. Total cross section σ_0 for the $I=0$ isotopic spin state for the K^+-N system.

For the K mesons the equation analogous to Eq. (12) is

$$\sigma_{Kd}=\text{“}\sigma_{Kp}\text{”}+\text{“}\sigma_{Kn}\text{”}-\delta\sigma\,, \tag{19}$$

where

$$\delta\sigma=\frac{\langle r^{-2}\rangle}{4\pi}\{2\text{“}\sigma_{Kp}\text{”}\,\text{“}\sigma_{Kn}\text{”}(1-\rho_p\rho_n) -\tfrac{1}{2}[\text{“}\sigma_{Kp}\text{”}^2(1-\rho_p{}^2)-\text{“}\sigma_{Kn}\text{”}^2(1-\rho_n{}^2)]\}\,. \tag{20}$$

Smooth curves, shown in Figs. 8 and 9, were first passed through the K^--p and K^--d data, and the Fermi momentum was folded into the K^--p curve according to (14). Both the folding and unfolding procedures previously outlined imply the knowledge of the total cross sections on hydrogen and deuterium targets well outside the momentum range covered in this experiment. For this purpose we have employed graphical interpolations of the data available in the literature.[16–23,30–36]

A curve for “σ_1”=“σ_{K^-n}” could then be computed from (19), and “σ_0” from

$$\text{“}\sigma_0\text{”}=2\text{“}\sigma_{K^-p}\text{”}-\text{“}\sigma_1\text{”}. \tag{21}$$

In (20), the value of $\langle r^{-2}\rangle$ was taken from the π-meson data, i.e., 0.0327 mb^{-1}. If the variation in $\langle r^{-2}\rangle$ is similar to the π-meson case, then by taking a constant $\langle r^{-2}\rangle$, the peaks in “σ_1” will tend to be slightly underestimated, whereas those in “σ_0” will tend to be overestimated. In any case, this effect should be small,

[30] A. N. Diddens, E. W. Jenkins, T. F. Kycia, and K. F. Riley, Phys. Rev. **132**, 2721 (1963).
[31] W. Galbraith, E. W. Jenkins, T. F. Kycia, B. A. Leontic, R. H. Phillips, A. L. Read, and R. Rubinstein, Phys. Rev. **138**, B913 (1965).
[32] W. F. Baker, E. W. Jenkins, T. F. Kycia, R. H. Phillips, A. L. Read, K. F. Riley, and H. Ruderman, in *Proceedings of the Sienna International Conference on Elementary Particles*, edited by G. Bernardini and G. P. Puppi (Società Italiana di Fisica, Bologna, Italy, 1963).
[33] W. F. Baker, R. L. Cool, E. W. Jenkins, T. F. Kycia, R. H. Phillips, and A. L. Read, Phys. Rev. **129**, 2285 (1963).
[34] G. von Dardel, D. H. Frisch, R. Mermod, R. H. Milburn, P. A. Piroué, M. Vivargent, G. Weber, and K. Winter, Phys. Rev. Letters **5**, 333 (1960).
[35] T. F. Kycia, L. T. Kerth, and R. G. Baender, Phys. Rev. **118**, 553 (1960).
[36] A. S. Vovenko *et al.*, Dubna Report No. D-721, 1961 (unpublished).

since the screening correction as computed from (20) tends to be small; typical values are listed in the last column of Table III.

Smooth curves for σ_0 and σ_1 were then obtained by unfolding according to (17) to the third iteration. In order to display more clearly the statistical significance of the results, "data points" and "statistical errors" were computed from these curves in the following manner. The "data points" for $I=0$ and $I=1$ were obtained by first computing the amount each K^--p and K^--d data point deviated from its smooth curve. These small deviations could then be used to compute a corresponding deviation for pure $I=0$ and $I=1$, neglecting the effects of Fermi motion and screening. The "data point" for $I=0$ or $I=1$ was then computed by adding this small deviation to the value given by the smooth $I=0$ or $I=1$ curve. The "data points" obtained by this method were found to be independent of any reasonable set of smooth curves which were used to compute them. The "statistical error" for each "data point" was computed using the assumptions that (1) the K^--p and K^--d errors were statistically independent, and (2) the second-order effects of Fermi motion and screening could be neglected. The results are shown in Fig. 16, and values are tabulated in Table VI.

One has an extra test of the folding and unfolding procedures, since the isotopic-spin relation for the K^--p total cross sections, Eq. (21), should be valid for both the folded and the unfolded cross sections. The final values obtained for σ_0 and σ_1, therefore, should be consistent with the K^--p data according to

$$\sigma_{K^-p}=\tfrac{1}{2}(\sigma_0+\sigma_1). \tag{22}$$

The agreement with (22) is reasonably satisfactory.

The K^+ data were analyzed in a similar manner. Smooth curves for the K^+-p and K^+-d cross sections, shown in Figs. 10 and 11, were fed in and the equations solved for "σ_{K^+n}". The smeared $I=0$ cross section was calculated as

$$\text{“}\sigma_0\text{”}=2\text{“}\sigma_{K^+n}\text{”}-\text{“}\sigma_{K^+p}\text{”} \tag{23}$$

and this was then unfolded to give σ_0 shown in Fig. 17. Values are tabulated in Table VII. From the same argument as before, the variation in $\langle r^{-2}\rangle$ will tend to underestimate the peak in "σ_{K^+n}" and hence, by (23), in "σ_0"; typical values of the screening correction computed from (20) are given in Table III. Moreover,

TABLE VII. K^+N total cross sections for the $I=0$ isotopic spin state. Also listed are the K^+-neutron total cross sections computed from $\sigma_T(K^+n)=\frac{1}{2}(\sigma_0+\sigma_1)$. Errors represent point-to-point statistical standard deviations. The over-all systematic error, including uncertainties in correcting for screening and Fermi motion in the deuteron, may be as high as $\pm 8\%$ for $I=0$ and $\pm 4\%$ for K^+n.

Laboratory momentum (GeV/c)	σ_0 (K^+N) (mb)	σ_T (K^+n) (mb)
0.888	19.31±1.35	16.85±0.52
0.939	19.62±1.13	17.60±0.45
0.989	21.09±0.94	18.53±0.36
1.040	20.42±0.89	18.91±0.35
1.091	24.09±0.89	20.61±0.35
1.141	24.40±0.54	21.25±0.21
1.191	23.27±0.43	20.87±0.17
1.242	21.97±0.42	20.26±0.16
1.292	20.74±0.39	19.68±0.15
1.342	20.20±0.38	19.32±0.16
1.392	20.17±0.38	19.22±0.16
1.442	20.09±0.36	19.07±0.14
1.492	19.98±0.34	18.95±0.13
1.593	19.83±0.31	18.79±0.12
1.643	19.48±0.24	18.67±0.10
1.693	19.53±0.22	18.69±0.08
1.743	19.96±0.22	18.88±0.08
1.793	19.65±0.22	18.73±0.08
1.893	19.18±0.22	18.50±0.08
1.993	19.50±0.29	18.55±0.11
2.093	19.82±0.29	18.67±0.11
2.193	19.26±0.31	18.40±0.13
2.393	19.71±0.29	18.63±0.11

TABLE VIII. Parameters of the observed structures as determined from fitting Breit-Wigner resonance functions. Although the total c.m. energy of each resonance is well determined by the fitting method, the results on the width and height depend sensitively on the type of background used. For the K^-N system a constant background was used: 26.0 mb for $I=0$ and 22.4 mb for $I=1$. For the K^+N system a smooth background which increased with energy but approached a constant asymptotically was assumed: a fourth-degree polynomial in $1/E$, where E is the total c.m. energy. *For these particular choices of background,* the statistical uncertainty was typically better than $\pm 30\%$ for the widths and $\pm 15\%$ for the heights.

Notation	S	I	Spin and parity	Laboratory momentum (GeV/c)	Total c.m. energy (MeV)	Full c.m. width (MeV)	Height (mb)	$4\pi\lambda^2$ (mb)	$(J+\frac{1}{2})x$	Elasticity x
$Y_0^*(1830)$	−1	0	$\frac{5}{2}^+$	1.07	1830±10	100	39.2	16.1	2.4	0.8
$Y_0^*(2107)$	−1	0	$\frac{7}{2}^-$	1.69	2107±10	185	13.6	8.6	1.6	0.4
$Y_0^*(2344)$	−1	0	$\frac{9}{2}^+$	2.28	2344±15	190	5.9	5.9	1.0	0.2
$Y_1^*(1770)$	−1	1	$\frac{5}{2}^-$	0.95	1770±10	100	21.2	19.3	1.1	0.4
$Y_1^*(1912)$	−1	1	$\frac{5}{2}^+$?	1.26	1912±10	30	2.8	12.8	0.22	0.07?
$Y_1^*(2025)$	−1	1	$\frac{7}{2}^+$	1.51	2025±10	165	4.7	10.0	0.47	0.12
$Y_1^*(2255)$	−1	1	$\frac{9}{2}^-$?	2.05	2255±10	170	2.8	6.7	0.42	0.08?
$Z_0^*(1780)$	+1	0	?	0.97	1780±10	565	18	18.7	0.95	?
$Z_1^*(1900)$	+1	1	?	1.23	1900±10	240	3.1	13.3	0.23	?

TABLE IX. Imaginary part squared of the forward elastic scattering amplitudes for the K^-N system. Results are given in mb/sr in the center-of-mass frame. They were computed from the measured total cross sections using the optical theorem, Eq. (26). Listed errors are the point-to-point statistical standard deviations. For a comparison with elastic scattering measurements, a systematic error of ±2% should be used.

Laboratory momentum (GeV/c)	K^-p (mb/sr)	Laboratory momentum (GeV/c)	K^-n (mb/sr)
0.969	9.44±0.32	0.966	7.07±0.41
0.975	9.54±0.32	0.972	7.26±0.37
1.022	12.08±0.20	1.019	5.86±0.19
1.080	12.70±0.14	1.077	5.57±0.14
1.116	10.19±0.13	1.113	4.59±0.12
1.130	10.17±0.09	1.127	4.27±0.08
1.169	8.57±0.11	1.166	4.28±0.11
1.179	8.59±0.07	1.176	4.28±0.07
1.220	7.47±0.08	1.217	4.80±0.08
1.230	7.52±0.04	1.227	4.69±0.07
1.270	6.63±0.07	1.267	5.12±0.08
1.283	6.72±0.04	1.280	5.12±0.05
1.320	6.37±0.06	1.317	4.86±0.06
1.336	6.52±0.03	1.333	4.79±0.04
1.370	6.81±0.05	1.367	5.04±0.06
1.384	6.83±0.04	1.381	5.41±0.04
1.434	7.51±0.04	1.431	5.85±0.05
1.488	8.40±0.04	1.485	6.20±0.05
1.509	8.90±0.04	1.506	6.20±0.04
1.549	9.51±0.06	1.546	6.34±0.05
1.583	9.89±0.05	1.580	6.34±0.05
1.637	10.28±0.05	1.634	6.20±0.05
1.687	10.55±0.04	1.684	6.06±0.05
1.735	10.53±0.04	1.732	6.26±0.05
1.785	10.32±0.04	1.782	6.22±0.05
1.835	10.22±0.05	1.837	6.42±0.05
1.840	10.03±0.05	1.876	6.76±0.05
1.879	10.08±0.05	1.882	6.90±0.05
1.885	10.10±0.05	1.926	7.30±0.05
1.929	10.19±0.05	1.982	7.59±0.06
1.985	10.34±0.04	2.032	7.78±0.05
2.035	10.55±0.04	2.077	8.05±0.05
2.080	10.77±0.04	2.121	8.33±0.05
2.124	11.00±0.04	2.161	8.41±0.05
2.164	11.25±0.05	2.203	7.94±0.05
2.206	11.58±0.05	2.237	7.82±0.06
2.240	11.74±0.06	2.298	8.18±0.05
2.250	11.81±0.12	2.348	8.45±0.12
2.301	12.01±0.05	2.389	8.66±0.06
2.351	12.13±0.12	2.420	8.92±0.07
2.392	12.13±0.06		
2.423	12.16±0.06		

since only iteration number 3 is used, the peak was probably not unfolded to its full height. Consequently, it is estimated that the peak in σ_0 is a lower limit.

VIII. DISCUSSION OF RESULTS

A. K^-N Total Cross Sections

The cross sections of definite isotopic spin are shown in Fig. 16 and tabulated in Table VI.

In the momentum range 0.9–2.4 GeV/c, the $I=0$ data show three enhancements at center-of-mass energies of 1830±10, 2107±10, and 2344±15. The $I=1$ curve shows four structures at center-of-mass energies of 1770±10, 1912±10, 2025±10, and 2255±10. Most of these structures have now been identified with hyperon resonances observed in production experiments.[37]

The $Y_0^*(1830)$ and $Y_1^*(1765)$ seem to be somewhat asymmetric and too large: One cannot exclude the presence of further structure in the mass region of 1820–1880 MeV.[37,38] A small structure in this mass region is difficult to study because it falls close to these two large peaks and is computed as the difference between two large numbers. A further complication may come from the fact that thresholds for reactions like $[K^*(890)N]$ and $[N^*(1236)K]$ fall in this same energy region.

A nonrelativistic Breit-Wigner formula is usually assumed for the shape of a resonance as a function of the total energy E in the center-of-mass system:

$$\sigma_T(E)=4\pi\lambda^2\frac{(J+\frac{1}{2})x}{[(E_R-E)2/\Gamma]^2+1}, \qquad (24)$$

where $\lambda=1/k=197.32/p_{\text{c.m.}}$, k is the wave number, $p_{\text{c.m.}}$ is the c.m. momentum, J and E_R are the angular momentum and the resonant energy, and x is the elasticity defined as

$$x=Y^*\rightarrow(\text{elastic channel})/Y^*\rightarrow(\text{all channels}). \qquad (25)$$

TABLE X. Imaginary part squared of the forward elastic scattering amplitudes for the K^+N system. Results are given in mb/sr in the center-of-mass frame. They were computed from the measured total cross sections using the optical theorem, Eq. (26). Listed errors are the point-to-point statistical standard deviations. For a comparison with elastic scattering measurements, a systematic error of ±2% should be used.

Laboratory momentum (GeV/c)	K^+p (mb/sr)	Laboratory momentum (GeV/c)	K^+n (mb/sr)
0.891	0.78±0.04	0.888	1.06±0.07
0.942	0.99±0.04	0.939	1.25±0.06
0.992	1.12±0.04	0.989	1.50±0.06
1.043	1.43±0.04	1.040	1.69±0.06
1.094	1.49±0.04	1.091	2.15±0.07
1.144	1.77±0.03	1.141	2.43±0.05
1.194	1.96±0.03	1.191	2.50±0.04
1.245	2.10±0.03	1.242	2.50±0.04
1.295	2.23±0.03	1.292	2.49±0.04
1.345	2.31±0.03	1.342	2.53±0.04
1.395	2.38±0.03	1.392	2.63±0.04
1.445	2.44±0.03	1.442	2.72±0.04
1.495	2.52±0.03	1.492	2.81±0.04
1.596	2.70±0.03	1.593	3.01±0.04
1.646	2.84±0.02	1.643	3.10±0.03
1.696	2.96±0.02	1.693	3.23±0.03
1.746	3.05±0.02	1.743	3.43±0.03
1.796	3.17±0.02	1.793	3.50±0.03
1.896	3.40±0.02	1.893	3.66±0.03
1.996	3.55±0.03	1.993	3.93±0.05
2.096	3.73±0.03	2.093	4.24±0.05
2.196	3.97±0.04	2.193	4.36±0.06
2.396	4.43±0.04	2.393	4.98±0.06

[37] N. Barash-Schmidt, A. Barbaro-Galtieri, L. R. Price, A. H. Rosenfeld, P. Söding, C. G. Wohl, and M. Roos, Rev. Mod. Phys. **41**, 109 (1969).

[38] R. Armenteros, M. Ferro-Luzzi, D. W. G. Leith, R. Levi-Setti, A. Minten, R. D. Tripp, H. Filthuth, V. Hepp, E. Kluge, H. Schneider, R. Barloutaud, P. Granet, J. Meyer, and J. P. Porte, Phys. Letters **24B**, 198 (1967); Nucl. Phys. **B3**, 592 (1967).

The energy dependence of Γ, the full width at half-maximum, is chosen as[39]

$$\Gamma=\Gamma_0\left(\frac{P_{\text{c.m.}}}{P_R}\right)^{2l+1}\left[\frac{E_R(A^2+P_R{}^2)}{E(A^2+P_{\text{c.m.}}{}^2)}\right]^l, \qquad (26)$$

where Γ_0 is the intrinsic width, P_R is the resonant c.m. momentum, $A=350$ MeV/c is an empirical constant, and l is the orbital angular momentum of the resonance.

The parameters of the structures, assuming they are resonances, were obtained by least-squares-fitting the $I=0$ and $I=1$ cross sections with the Breit-Wigner formula (24) plus a smooth background described by a polynomial of the center-of-mass energy. The parameters to be determined were E_R, Γ, $[(J+\frac{1}{2})x]$, and the coefficients of the background. An available IBM 7094 computer program was adapted to this purpose.[40] A second computer program which subtracts one bump at a time was also used. In this case the parameters of the Breit-Wigner formula were varied so as to obtain a background as smooth as possible after subtracting all the structures.

Two hypotheses are necessary for this analysis procedure: (a) The structures are describable by a Breit-Wigner formula of the type given in Eq. (24); (b) the nonresonant background is a smooth function of the energy in the center-of-mass system. Though these assumptions are reasonable, they must be regarded as first-order approximations. Moreover, it is well known that some total cross-section structures are due to several resonant states, so that several overlapping Breit-Wigner formulas should be used. We have used the $I=0$ states 1670, 1690, 1830, and 1865, and the $I=1$ states 1660 and 1700 as determined from other experiments.[37] Also, inelastic channel thresholds in the region of the bumps may make the background vary rapidly with energy. Finally, the procedure for extracting the pure isospin cross sections from the deuteron data may distort some of the features.

Bearing these limitations in mind, the results of such Breit-Wigner fittings to the total cross-section structures are given in Table VIII, below. The goodness of the fit, as given by the sum of the deviations squared (χ^2) divided by the number of degrees of freedom, is, in general, adequate. It is only after fitting the structures with Breit-Wigner formulas that one finds the considerable overlapping among resonances and that the observed structures are sometimes only the tops of the resonances.

Hyperon resonances with large masses have been previously reported in the literature. Böck *et al.*[41] at CERN, with limited statistics, reported *narrow* hyperon resonances at 1942±9, 2097±6, and 2299±6 MeV in $\bar{Y}Y^*$ final states in a hydrogen-bubble-chamber exposure to 5.7-GeV/c $\bar{p}$. The first structure should have isotopic spin $I=1$, while the isospins of the others were not determined. Blanpied *et al.*,[42] with limited statistics, reported hyperon resonances of unknown isospin at 2022±20 and 2245±25 MeV in the photoproduction of K^+ mesons. It is difficult to reconcile these masses and widths with ours, within their stated errors.

Wohl *et al.*,[43] from a detailed analysis of the angular distributions in $K^-p\to\bar{K}^0n$ and $K^-p\to\Lambda^0\pi^0$ as func-

TABLE XI. Imaginary part squared of the forward charge-exchange scattering amplitudes for the K^-N and K^+N systems. Results are given in mb/sr, in the center-of-mass frame. They were computed from the measured total cross sections using the optical theorem, Eq. (27). Statistical point-to-point errors are listed; the systematic error dominates and is about ±0.5 mb/sr for K^-N and ±0.05 mb/sr for K^+N.

Laboratory momentum (GeV/c)	K^-N (mb/sr)	Laboratory momentum (GeV/c)	K^+N (mb/sr)
0.966	0.3 ±0.2	0.891	0.05±0.03
0.972	0.3 ±0.2	0.942	0.03±0.02
1.019	2.2 ±0.3	0.992	0.06±0.03
1.077	3.0 ±0.2	1.043	0.02±0.02
1.113	2.3 ±0.2	1.094	0.12±0.04
1.127	2.6 ±0.2	1.144	0.11±0.02
1.166	1.5 ±0.2	1.194	0.07±0.02
1.176	1.5 ±0.1	1.245	0.04±0.01
1.217	0.61±0.07	1.295	0.02±0.01
1.227	0.69±0.05	1.345	0.01±0.01
1.267	0.21±0.04	1.395	0.01±0.01
1.280	0.22±0.02	1.445	0.02±0.01
1.317	0.21±0.03	1.495	0.02±0.01
1.333	0.26±0.02	1.596	0.02±0.01
1.367	0.26±0.03	1.646	0.01±0.01
1.381	0.16±0.02	1.696	0.01±0.01
1.431	0.20±0.02	1.746	0.02±0.01
1.485	0.32±0.03	1.796	0.02±0.01
1.506	0.47±0.03	1.896	0.01±0.01
1.546	0.63±0.04	1.996	0.02±0.01
1.580	0.77±0.04	2.096	0.03±0.01
1.634	1.02±0.05	2.196	0.02±0.01
1.684	1.24±0.05	2.396	0.03±0.01
1.732	1.11±0.05		
1.782	1.03±0.05		
1.837	0.88±0.04		
1.876	0.66±0.04		
1.882	0.61±0.04		
1.926	0.48±0.03		
1.982	0.42±0.03		
2.032	0.42±0.03		
2.077	0.39±0.03		
2.121	0.36±0.03		
2.161	0.41±0.03		
2.203	0.68±0.04		
2.237	0.79±0.05		
2.298	0.73±0.04		
2.348	0.66±0.09		
2.389	0.58±0.04		
2.420	0.50±0.04		

[39] J. D. Jackson, Nuovo Cimento **34**, 1644 (1964).
[40] E. A. Crosbie, AN-E208 (unpublished); M. A. Mariscotti, BNL Report No. 10441 (unpublished).
[41] R. K. Böck, W. A. Cooper, B. R. French, F. B. Kinson, R. Levi-Setti, D. Revel, B. Tallini, and S. Zylberajch, Phys. Letters **17**, 166 (1965).
[42] W. A. Blanpied, J. S. Greenberg, V. W. Hughes, P. Kitching, D. C. Lu, and R. C. Minehart, Phys. Rev. Letters **14**, 741 (1965).
[43] C. W. Wohl, F. T. Solmitz, and M. L. Stevenson, Phys. Rev. Letters **17**, 107 (1966).

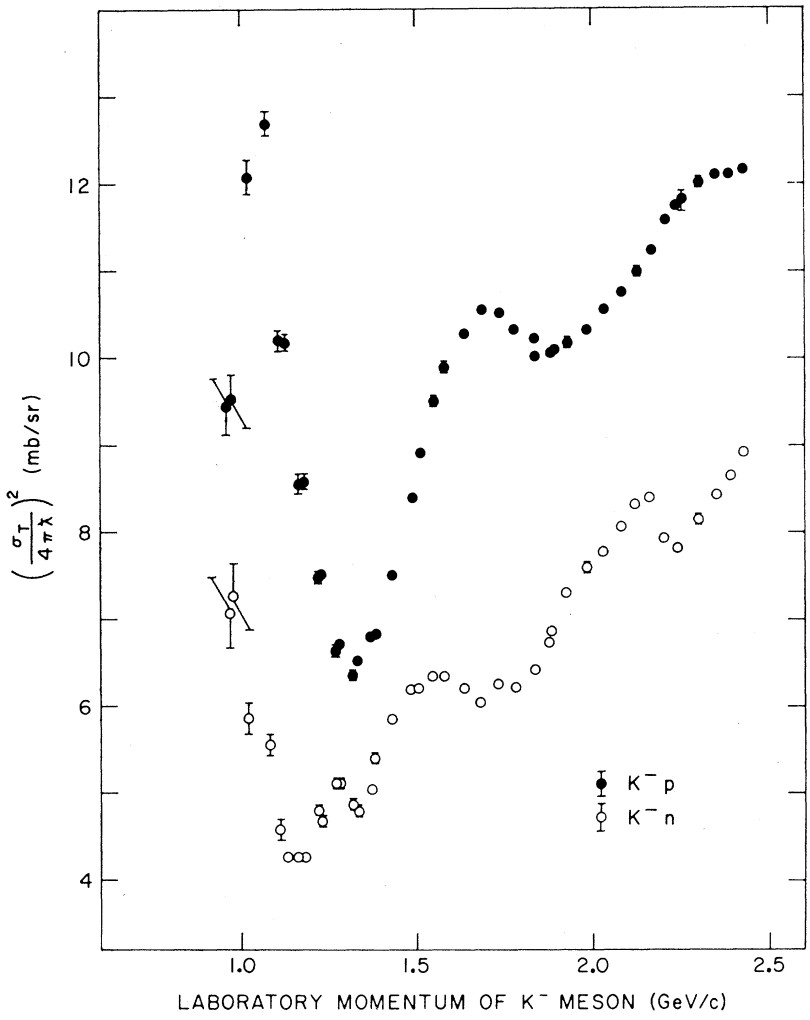

FIG. 18. Imaginary parts squared of the forward elastic scattering amplitudes for K^--p and K^--n.

tions of incoming momentum, were able to determine the spin and parity of $Y_1^*(2025)$ as $\frac{7}{2}^+$ and of $Y_0^*(2107)$ as $\frac{7}{2}^-$. Independent confirmation of the existence and/or of the spin-parity assignment of the $Y_1^*(2025)$ comes from other bubble-chamber experiments.[37] As for the $Y_1^*(1912)$, though not necessarily required by the data of Wohl *et al.*,[43] Smart *et al.*,[44] and Armenteros *et al.*,[38] it is in the correct direction for improving their analyses.

Recent confirmation of the $Y_1^*(1912)$ and of the $Y_1^*(2255)$ come from a production-bubble-chamber experiment in the final state $\Sigma^0\pi^+\pi^-$ (3- to 4-standard-deviation effects).[45]

The structures reported in the present experiment could be classified as Regge recurrences as follows:

(1) The $Y_0^*(2107)$ with $J^P=\frac{7}{2}^-$ may be a recurrence of the $Y_0^*(1520)$.

(2) The $Y_0^*(2344)$ may be the second recurrence of the Λ and thus have an assignment of $\frac{9}{2}^+$.

(3) The $Y_1^*(1912)$ is probably a $\frac{5}{2}^+$ state and could be the recurrence of the Σ.

(4) The $Y_1^*(2025)$ with $J^P=\frac{7}{2}^+$ could be the recurrence of the $Y_1^*(1383)$.

(5) The $Y_1^*(2255)$ could be the recurrence of either the $Y_1^*(1765)$ or of the $Y_1^*(1660)$. In the first case it would have $J^P=\frac{9}{2}^-$.

From the point of view of unitary-symmetry classifications:

The $Y_1^*(1912)$ could be the missing member of the $\frac{5}{2}^+$ baryon octet together with $N_{1/2}^*(1688)$, $Y_0^*(1815)$, and the recently discovered $\Xi^*(2030)$. The mass formula is roughly satisfied [up to a few tens of MeV for $\Xi^*(2030)$].

The $Y_1^*(2025)$ could be a member of a $\frac{7}{2}^+$ recurrence of the decuplet together with $N_{3/2}^*(1924)$.

[44] W. M. Smart, A. Kernan, G. E. Kalmus, and R. P. Ely, Phys. Rev. Letters **17**, 556 (1966).

[45] V. E. Barnes, E. Flaminio, L. Montanet, N. P. Samios, I. O. Skillicorn, M. Goldberg, and K. Jaeger, Phys. Rev. Letters **22**, 479 (1969).

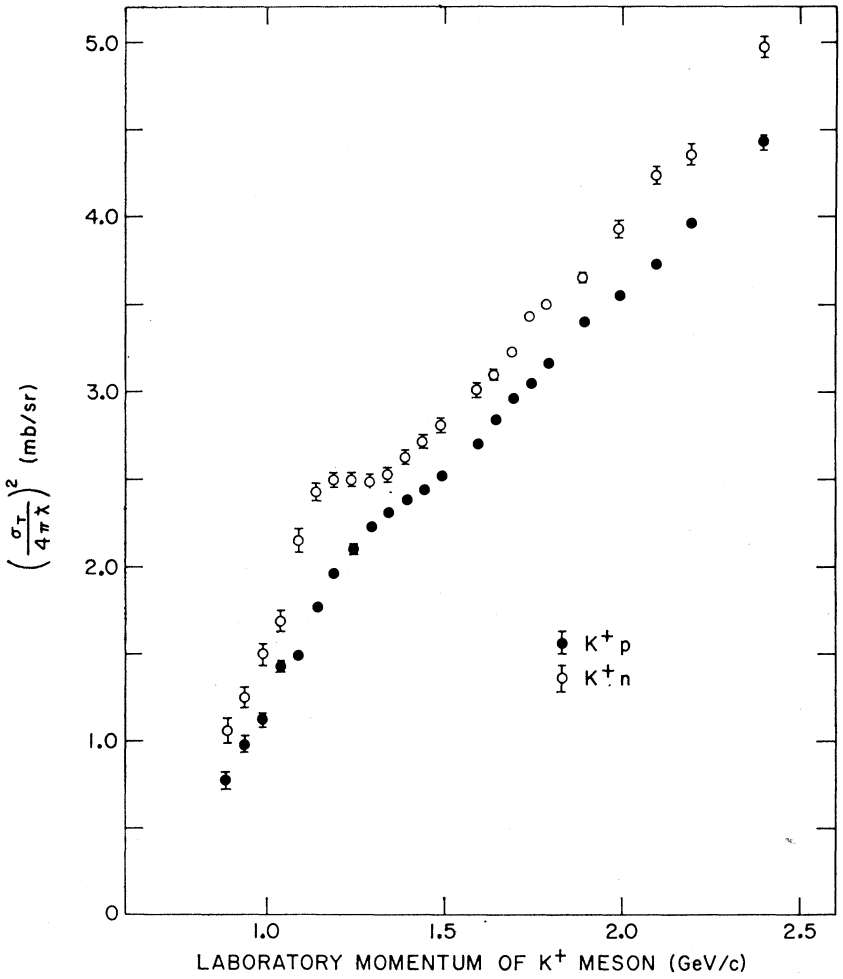

FIG. 19. Imaginary parts squared of the forward elastic scattering amplitudes for K^+-p and K^+-n.

The $Y_0^*(2107)$ could start a new octet with the $N_{1/2}^*(2190)$.

B. K^+N Total Cross Sections

The pure $I=1$ and $I=0$ cross sections are shown in Figs. 10 and 17, respectively, and tabulated in Tables V and VII.

The $I=1$ cross section has one structure, which does not have the appearance of a symmetric bump, at a laboratory momentum of 1.25 GeV/c. The results of a Breit-Wigner fitting, similar to that described for K^-N, are tabulated in Table VIII. The same limitations discussed for the K^-N system apply here as well.

Bubble-chamber data[3,46–52] indicate that the rise in the $I=1$ cross section above 650 MeV/c is connected with the increase in the one-pion production cross section, which remains small until the $N_{33}^*(1236)$ threshold is reached. In this region there is a sharp increase, and most of the one-pion production goes via the $N_{33}^*(1236)$ resonance. The production angular distributions of the N_{33}^* in the K^+-p center-of-mass frame is peaked backward; the KN_{33}^* final state is equally divided between $P_{1/2}$ and $P_{3/2}$ final states,[52] which is more characteristic of a vector-meson exchange mechanism than of a resonance state decaying into N_{33}^*K.

---

[46] J. L. Brown, R. W. Bland, M. G. Bowler, G. Goldhaber, S. Goldhaber, A. H. Hirata, J. A. Kadyk, V. H. Seeger, and G. H. Trilling, UCRL Report No. UCRL-11446, 1964 (unpublished).

[47] G. B. Chadwick, D. J. Crennell, W. T. Davies, M. Derrick, J. H. Mulvey, P. B. Jones, D. Radojicic, C. A. Wilkinson, A. Bettini, M. Cresti, S. Limentani, L. Peruzzo, and R. Santangelo, Phys. Letters **6**, 309 (1963).

[48] B. Kehoe, Phys. Rev. Letters **11**, 93 (1963).

[49] E. Boldt, J. Duboc, N. H. Duong, P. Eberhard, R. George, V. P. Henri, F. Levy, J. Poyen, M. Pripstein, J. C. Crussard, and A. Tran, Phys. Rev. **133**, B220 (1964).

[50] M. Ferro-Luzzi, R. George, Y. Goldschmidt-Clermont, V. P. Henri, B. Jongejans, D. W. G. Leith, G. R. Lynch, F. Muller, and J. M. Perreau, Nuovo Cimento **36**, 1101 (1965).

[51] R. W. Bland, M. G. Bowler, J. L. Brown, G. Goldhaber, S. Goldhaber, V. H. Seeger, and G. H. Trilling, Phys. Rev. Letters **18**, 1077 (1967).

[52] R. D. Tripp, in *Proceedings of the Fourteenth International Conference on High-Energy Physics, Vienna, 1968* (CERN, Geneva, 1968), p. 173.

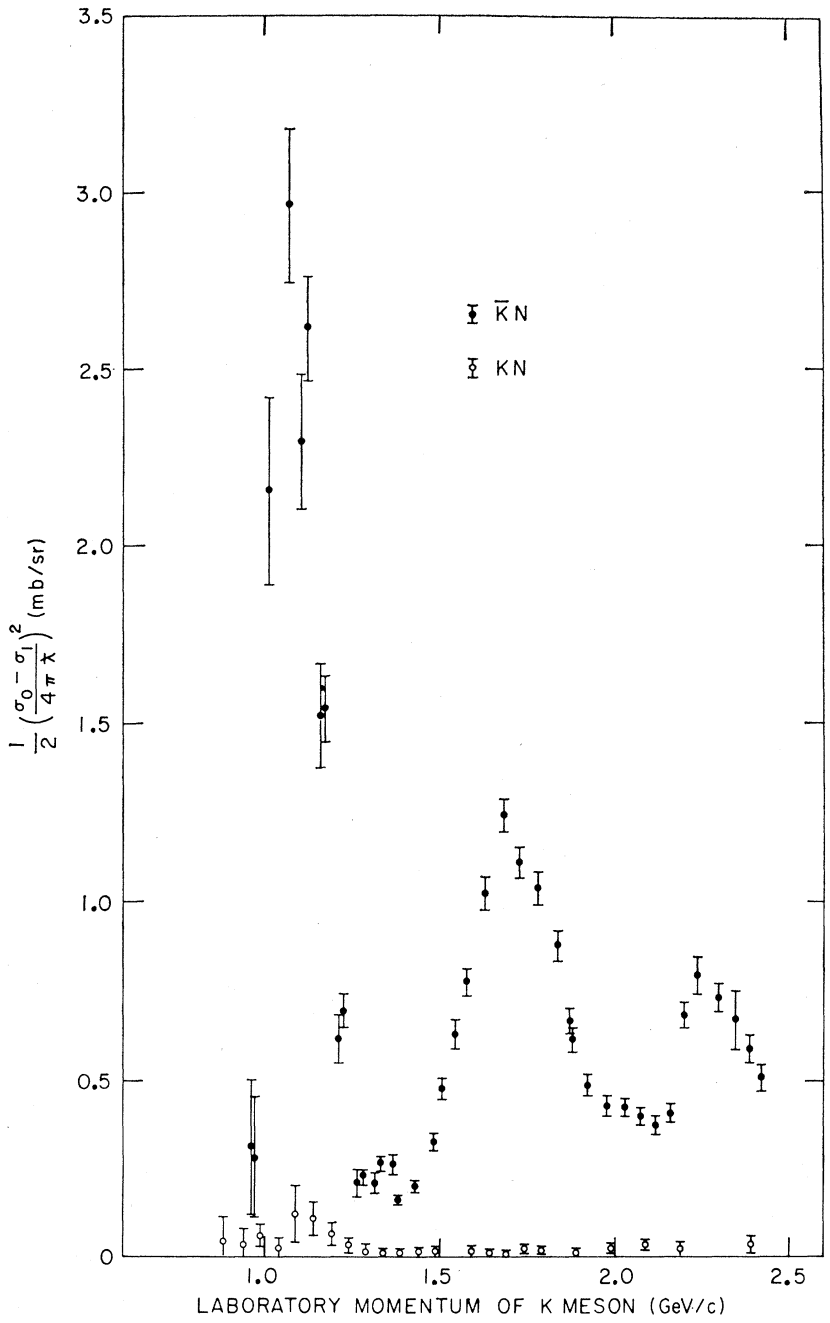

FIG. 20. Imaginary parts squared of the forward elastic scattering amplitudes for π^--p and π^+-p.

Phase-shift analyses of K^+-p data[53,54] indicated several possible solutions, one of which showed possible evidence for a P_{11}, $S=+1$, $I=1$ resonance at a mass of 2 GeV. Included in the analysis are recent K^+-p backward scattering data which exhibit some structure.[55] Phase-shift analyses from more recent K^+-p polarization data at 1.22 and 2.48 GeV/c favor the solution which requires no resonance in the K^+-p system.[56]

In the original analysis of our $I=0$ data (Fig. 17) above 0.9 GeV/c,[3] only one structure was observed in $I=0$ at about 1.25 GeV/c. It was interpreted by

[53] A. T. Lea, B. R. Martin, and C. C. Oades, Phys. Letters **23**, 380 (1966); Phys. Rev. **165**, 1770 (1968).
[54] B. R. Martin, Phys. Rev. Letters **21**, 1286 (1968).
[55] A. S. Carroll, J. Fischer, A. Lundby, R. H. Phillips, C. L. Wang, F. Lobkowicz, A. C. Melissinos, Y. Nagashima, and S. Tewksbury, Phys. Rev. Letters **21**, 1282 (1968).
[56] S. Andersson, C. Daum, F. C. Erne, J. P. Lagnaux, J. C. Sens, and F. Udo (unpublished).

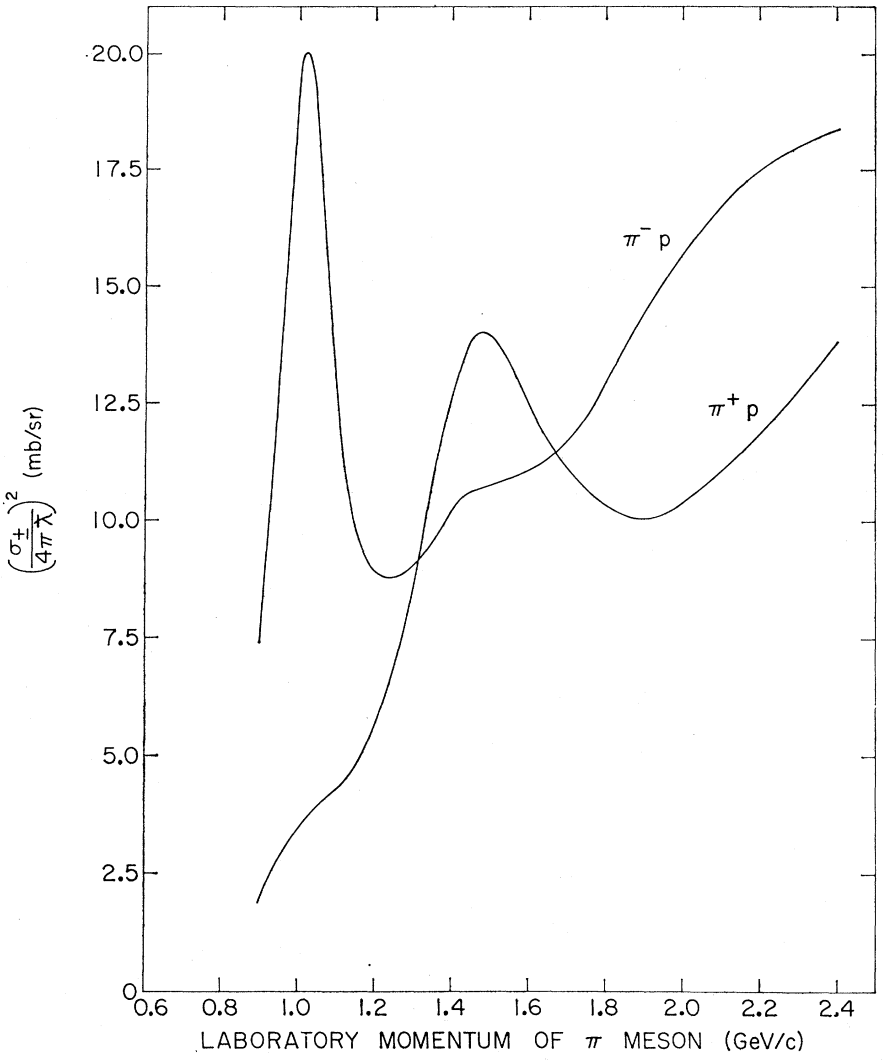

FIG. 21. Imaginary parts squared of the forward charge-exchange scattering amplitudes for $K^-+p\to\bar{K}^0+n$ and $K^++n\to K^0+p$.

Krammer and Lomon[57] as being due to a threshold effect for K^* production. Another explanation was that it arises from a rising $I=0$ K^*N cross section superimposed on a smoothly decreasing elastic cross section.[58] The reanalysis included here makes use of the new data below 0.9 GeV/c on K^+-N total[21] and inelastic[58] cross sections. It indicates the existence of a new structure in $I=0$ at 790 MeV/c.[59] The double-peaked structure revealed by the reanalysis can be interpreted as an elastic peak at 790 MeV/c together with a rapidly rising K^*N cross section. Should the lower peak be due to a K^+-N resonance in $I=0$, it would have the parameters $M=1780$ MeV, $\Gamma_0\cong 565$ MeV, and $(J+\frac{1}{2})\chi\simeq 0.95$. The fit would be best for an $l=1$, $J=\frac{1}{2}$, almost elastic resonance.

In the momentum region below 1.4 GeV/c, the inelastic processes for the $I=0$ system are considerably different from those for the $I=1$ system, mainly because the $N_{33}{}^*K$ state is not allowed for σ_0. Relevant processes for the $I=0$ state, like K^+-N elastic scattering and charge exchange, have been studied in deuterium bubble chambers.[46–50] The phase-shift analysis of the data, using the impulse approximation, requires SP and probably SPD waves. Two sets of phases corresponding to the Fermi-Yang ambiguity best fit the data. A dispersion relation calculation[60–62] favors the Yang set, which has rapidly rising $I=0$ $S_{1/2}$ and $P_{1/2}$ positive phase shifts. It is difficult to extrapolate this

[57] M. Krammer and E. L. Lomon, Phys. Rev. Letters **20**, 71 (1968).
[58] A. A. Hirata, C. G. Wohl, G. Goldhaber, and G. H. Trilling, Phys. Rev. Letters **21**, 1485 (1968).
[59] R. J. Abrams, R. L. Cool, G. Giacomelli, T. F. Kycia, K. K. Li, and D. N. Michael, Phys. Letters **30B**, 564 (1969).
[60] R. L. Warnock and G. Frye, Phys. Rev. **138**, B947 (1965).
[61] C. Lovelace, CERN Report No. TH 628, 1965 (unpublished).
[62] W. J. Debonte and E. L. Lomon, Nuovo Cimento **44**, A647 (1966).

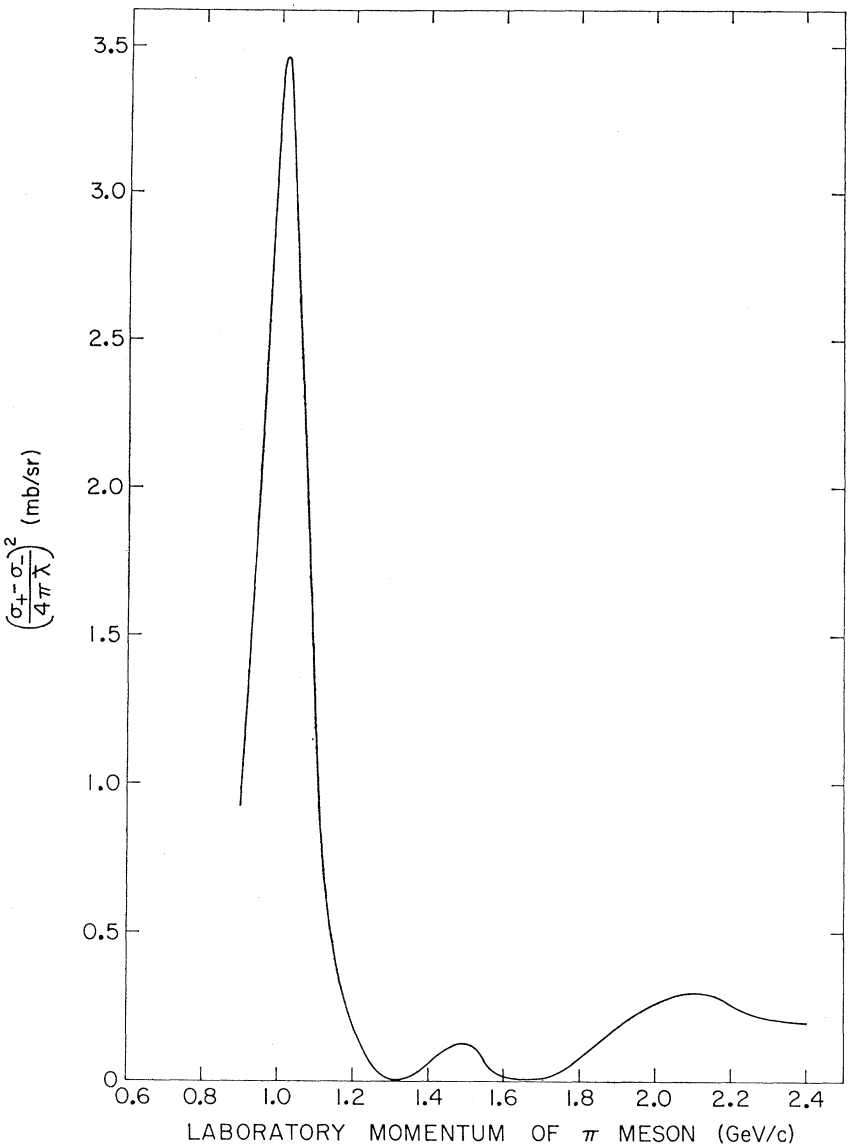

FIG. 22. Imaginary part squared of the forward charge-exchange scattering amplitude for $\pi^- + p \to \pi^0 + n$.

result to the region of the $I=0$ structure, because of the large extrapolation required.[47,48]

If it is a resonance, the only $SU(3)$ representation possible for this $Y=2$ state is an antidecuplet.

C. Imaginary Parts of Forward Scattering Amplitudes

For completeness we compute the imaginary parts of the forward elastic and charge-exchange scattering amplitudes as derived via the optical theorem:

$$|\mathrm{Im}f_{\mathrm{el}}(0)|^2=(\sigma_T/4\pi\lambda\!\!\!^{-})^2. \tag{27}$$

For K mesons,

$$|\mathrm{Im}f_{\mathrm{ch.ex.}}(0)|^2=\tfrac{1}{2}[(\sigma_0-\sigma_1)/4\pi\lambda\!\!\!^{-}]^2; \tag{28}$$

for π mesons,

$$|\mathrm{Im}f_{\mathrm{ch.ex.}}(0)|^2=\tfrac{1}{2}[(\sigma_+-\sigma_-)/4\pi\lambda\!\!\!^{-}]^2. \tag{29}$$

These quantities are given in Tables IX–XI and are shown in Figs. 18–22. Elastic scattering and charge-exchange differential distributions in the momentum region covered by this experiment are either not precise enough or do not go to small enough angles to make a meaningful direct estimate of the forward real parts.

IX. CONCLUSIONS

Several new enhancements have been found in this total cross-section measurement. Table VIII summarizes their properties. A few comments can be made on these results.

(a) The K^-N total cross sections in the 0.9–2.4-GeV/c region exhibit many structures, which are interpreted as hyperon resonances.

(b) The K^+N total cross sections exhibit at least two structures, one in each isotopic spin state. A conclusive interpretation is at present not possible.

(c) The analysis of the π-meson data throws some light on and points out the limitations of the analysis of experimental data using neutron targets bound in the deuteron.

(d) The availability of a reasonably intense and pure K-meson beam makes the precise measurement of total cross sections a powerful tool for investigating the existence and determining some of the properties of strange-baryon resonances.

(e) Of the above-mentioned new structures, the Y_0^* (2107), Y_1^* (1912), Y_1^* (2025), Z_1^* (1900), and Z_0^* (1780) have already been confirmed by independent measurements.[19,21,42,43]

ACKNOWLEDGMENTS

We wish to thank Dr. G. K. Green, Dr. J. R. Sanford, T. Blair, and the AGS staff for their support. We thank Dr. A. Ashmore, Dr. A. Mueller, Dr. R. Peierls, and Dr. L. Stodolsky for useful discussions and Dr. R. J. Abrams and Dr. D. N. Michael for their assistance in data analysis. The cooperation of A. P. Schlafke and the Cryogenic Group is greatly appreciated. We also wish to acknowledge the aid of J. Fuhrmann and the technical assistance of P. Anzoli, G. Munoz, H. Sauter, F. Seier, and O. Thomas.

PHYSICAL REVIEW D VOLUME 1, NUMBER 7 1 APRIL 1970

Total Cross Sections of $K^{\pm}$ Mesons and Antiprotons on Nucleons up to 3.3 GeV/c†

R. J. Abrams, R. L. Cool, G. Giacomelli,* T. F. Kycia, B. A. Leontic,‡ K. K. Li, and D. N. Michael
Brookhaven National Laboratory, Upton, New York 11973

(Received 8 October 1969)

Total cross sections of $K^{\pm}$ and $\bar{p}$ on hydrogen and deuterium were measured in a standard transmission experiment with statistical precisions of the order of 0.05–0.25%. Data were obtained in the momentum range 2.45–3.30 GeV/c for K^-N, 1.55–3.30 GeV/c for K^+N, and 1.00–3.30 GeV/c for $\bar{p}N$. Cross sections for the pure isotopic spin states are obtained using a procedure for the deuterium data which takes into account Fermi motion and the shadow effect. Evidence for the following new structures was found: $Y_1^*(2455)$, $Y_1^*(2620)$, $Y_0^*(2585)$, $Z_1^*(2150)$, $Z_1^*(2500)$, $\pi_1^*(2190)$, $\pi_1^*(2350)$, and $\pi_0^*(2375)$.

I. INTRODUCTION

MEASUREMENTS of kaon-nucleon total cross sections have been performed with high enough precision to detect several new strange-baryon resonances.[1–4] The availability of partially separated beams of sufficient purity and intensity has made it possible to extend these measurements to higher energy as well as to perform new measurements of antiproton-nucleon total cross sections. In the present paper we describe a search for higher-mass baryon resonances with strangeness ± 1 and for high-mass nonstrange boson resonances using the total cross-section method.

In this experiment, the total cross sections were measured in hydrogen and deuterium with K^- mesons from 2.45 to 3.30 GeV/c laboratory momentum, with K^+ mesons from 1.55 to 3.30 GeV/c, and with antiprotons from 1.00 to 3.30 GeV/c. The measurements were performed at 50-MeV/c intervals with a point-to-point statistical accuracy ranging from 0.05 to 0.25%. Preliminary results of the experiment have already been published.[2–4]

In searching for new resonances, the total cross section is the least sensitive formation experiment, but it can be carried out to a very high statistical accuracy which compensates for its poor intrinsic sensitivity. If a structure is found, the measurement can yield information on the mass, isotopic spin, width, and height from which one obtains the product of spin and elasticity.[1] The interpretation of a structure in the total cross section, however, is not unique: it could be the result of a resonance or a threshold effect.

We shall give the description of the experiment in Sec. II, corrections and uncertainties in the data in Sec. III, and the experimental results in Sec. IV. Throughout the present paper, we shall refer to I[1] for

† Work performed under the auspices of the U. S. Atomic Energy Commission.

* On leave of absence from the University of Bologna, Bologna, Italy.

‡ Present address: Institut za Fiziku Sveucilista, Zagreb, Yugoslavia.

[1] R. L. Cool, G. Giacomelli, T. F. Kycia, B. A. Leontic, K. K. Li, A. Lundby, J. Teiger, and C. Wilkin, preceding paper, Phys. Rev. D 1, 1887 (1970). This paper is referred to throughout the text as I.

[2] R. J. Abrams, R. L. Cool, G. Giacomelli, T. F. Kycia, B. A. Leontic, K. K. Li, and D. N. Michael, Phys. Rev. Letters 18, 1209 (1967).

[3] R. J. Abrams, R. L. Cool, G. Giacomelli, T. F. Kycia, B. A. Leontic, K. K. Li, and D. N. Michael, Phys. Rev. Letters 19, 259 (1967).

[4] R. J. Abrams, R. L. Cool, G. Giacomelli, T. F. Kycia, B. A. Leontic, K. K. Li, and D. N. Michael, Phys. Rev. Letters 19, 678 (1967).